CHAPTER IV

RESULTS AND DISCUSSION

4.1   Characterization

4.1.1 UV-Visible Spectroscopy.

UV-Vis spectra were determined in order to illustrate the optical properties that are important for the conductive polymer. The optical properties of the conductive polymer are generally considered in terms of absorption wavelength, which can be converted to photon energy in electron volt units by using Einstein's equation as:

$$E = h\nu = \frac{hc}{\lambda} \qquad (4.1)$$

where: E is photon energy (J), h is Plank's constant which is equal to 6.62×10^{34} J-sec, ν is the frequency (Hz or sec^{-1}), c is the light velocity in vacuum, which is equal to 3×10^{8} m/sec and λ is the wavelength (m) of the light.

Samples of undoped polyaniline (emeraldine base, EB) was prepared by dissolving 0.1 g of polyaniline powder in 1000 ml of NMP solution. The absorption spectra of EB are shown in Figure 4.1 The spectrum of undoped polyaniline shows two adsorption peaks at 324 and 633 nm due to the π-π* transition of benzenoid ring (Sertova et al.,1998) and the excitation of quinoid ring (Wan et al.,1992), respectively.
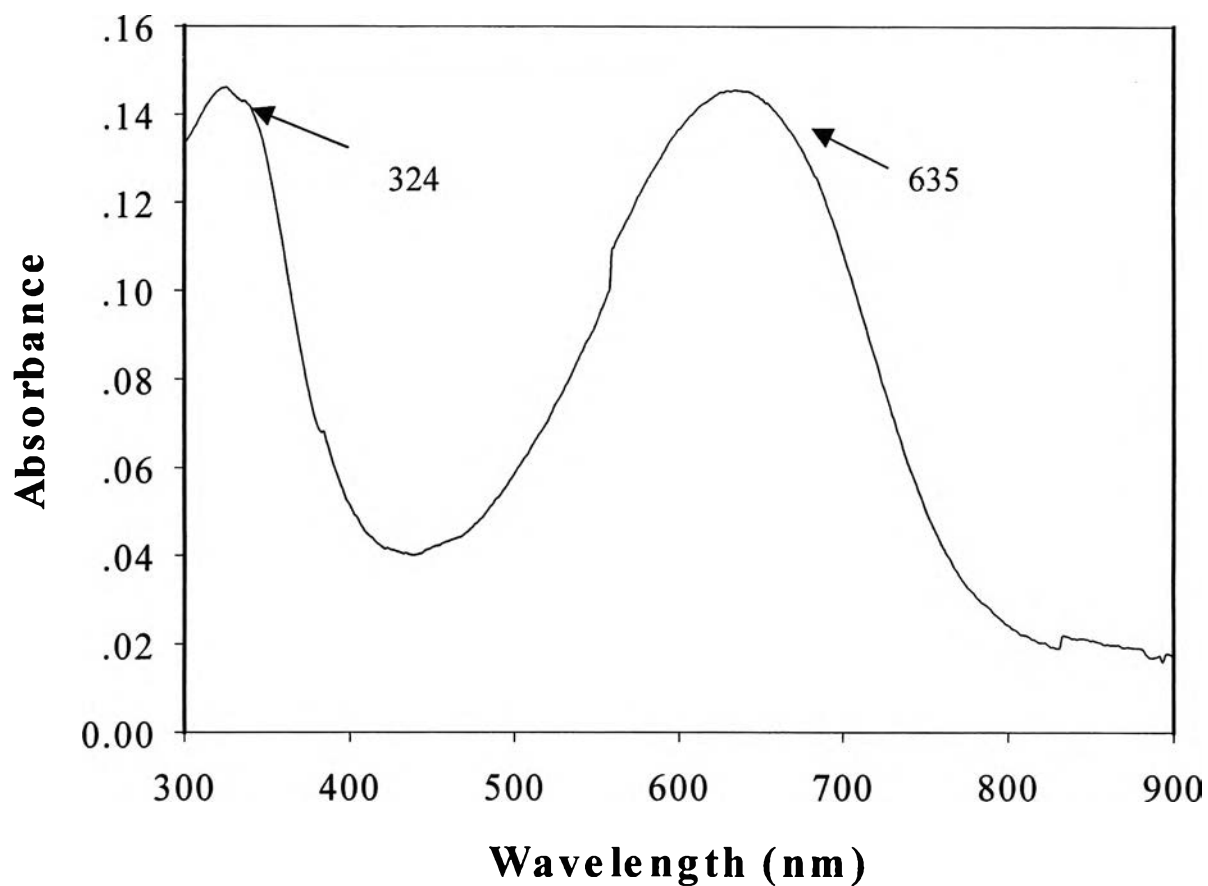
Figure 4.1 UV-Vis spectrum of emeraldine base (EB).

In order to study the effect of dopant type and doping level, the emeraldine base (EB) was doped with different acid dopants and at different doping levels. When EB was doped, N atoms on the imine site were protonated resulting in semiquinoid radical cations (Furukawa *et al.*, 1988). This caused decreases in the excitation absorption intensity peaks at 324 and 633 nm. Two new absorption peaks around 450 and 700-800 nm appear. The two absorption peaks represent the bipolaron and polaron states, indicative the conducting behavior of the polymer (Zeng *et al.*, 1992).

The spectra of doped-polyaniline are shown in Figures 4.2-4.4. The assignments of UV-Visible are tabulated in the Tables 4.1 and 4.2. The absorption spectrum of polyaniline doped with CSA (PANI-H_2SO_4/CSA) has the farthest red shift, going from 633 to 787 nm. When N_A/N_{EB} was increased, the spectra showed the same peak. This suggests that PANI-H_2SO_4/CSA has already reached the saturated state. In the case of polyaniline doped with HNO_3 (PANI-H_2SO_4/HNO_3) and polyaniline doped with HCOOH (PANI-H_2SO_4/HCOOH), the spectra peaks shifted when N_A/N_{EB} was increased. This was because N atoms on the imine sites were partially protonated at low doping levels. Unexpectedly, for PANI-H_2SO_4/HCOOH at N_A/N equal to 1:400, the absorption peak has a blue shift from 697 to 648 nm. This was due to N atoms on the imine sites deprotonated, resulting in a lower proportion of bipolaron/polaron state.
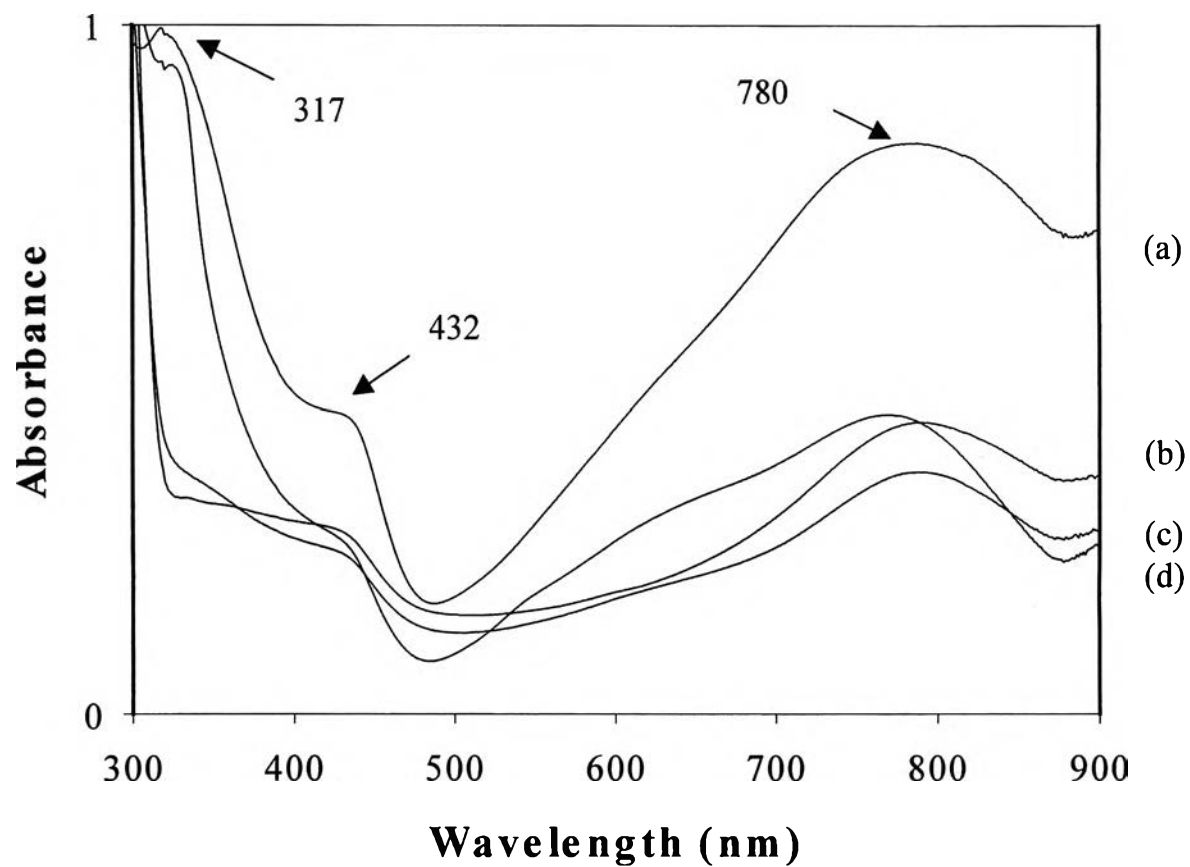
Figure 4.2 UV-Vis spectra of PANI-H$_2$SO$_4$/CSA at N$_{EB}$/N$_A$ of : (a) 1: 4; (b) 1: 40; (c) 1: 200 ; and (d) 1: 400.
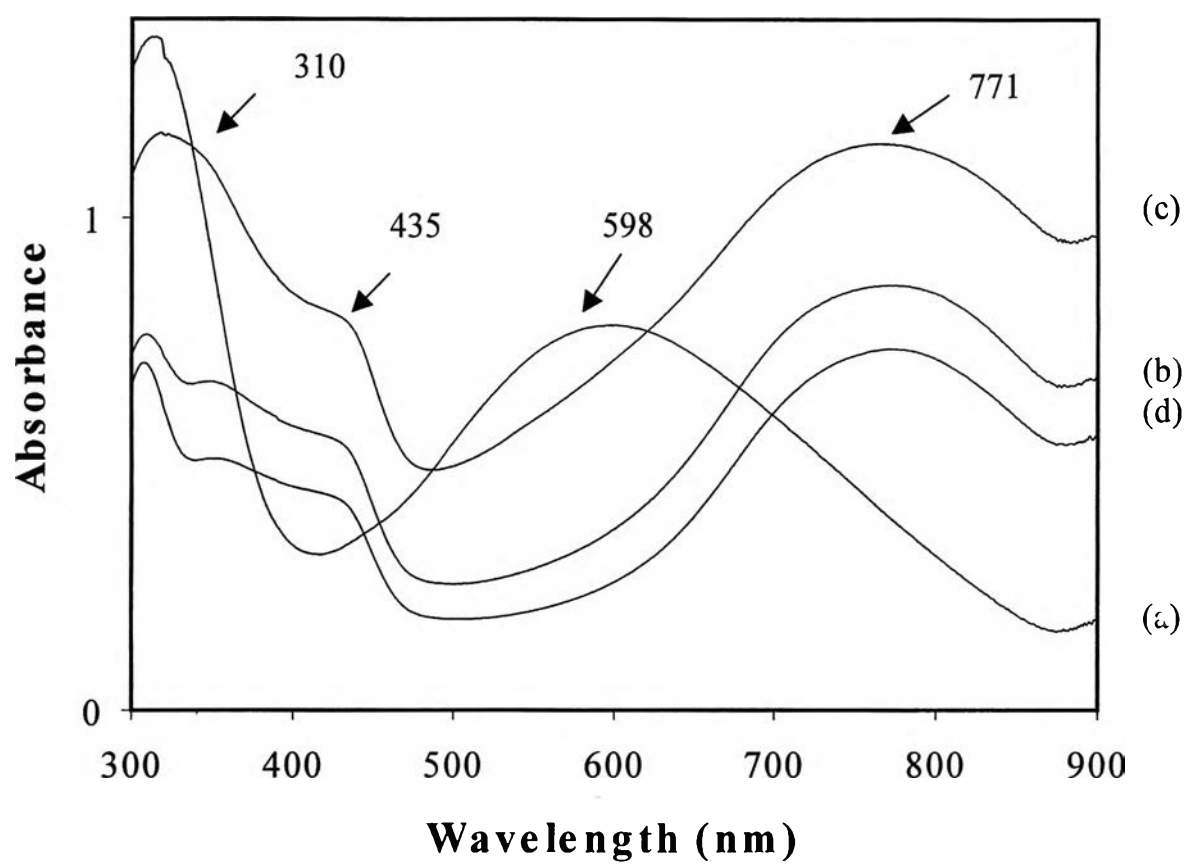
Figure 4.3 UV-Vis spectra of PANI-H$_2$SO$_4$/HNO$_3$ at N$_{EB}$/N$_A$ of: (a) 1: 4 ; (b) 1: 40; (c) 1: 200; and (d) 1: 400.
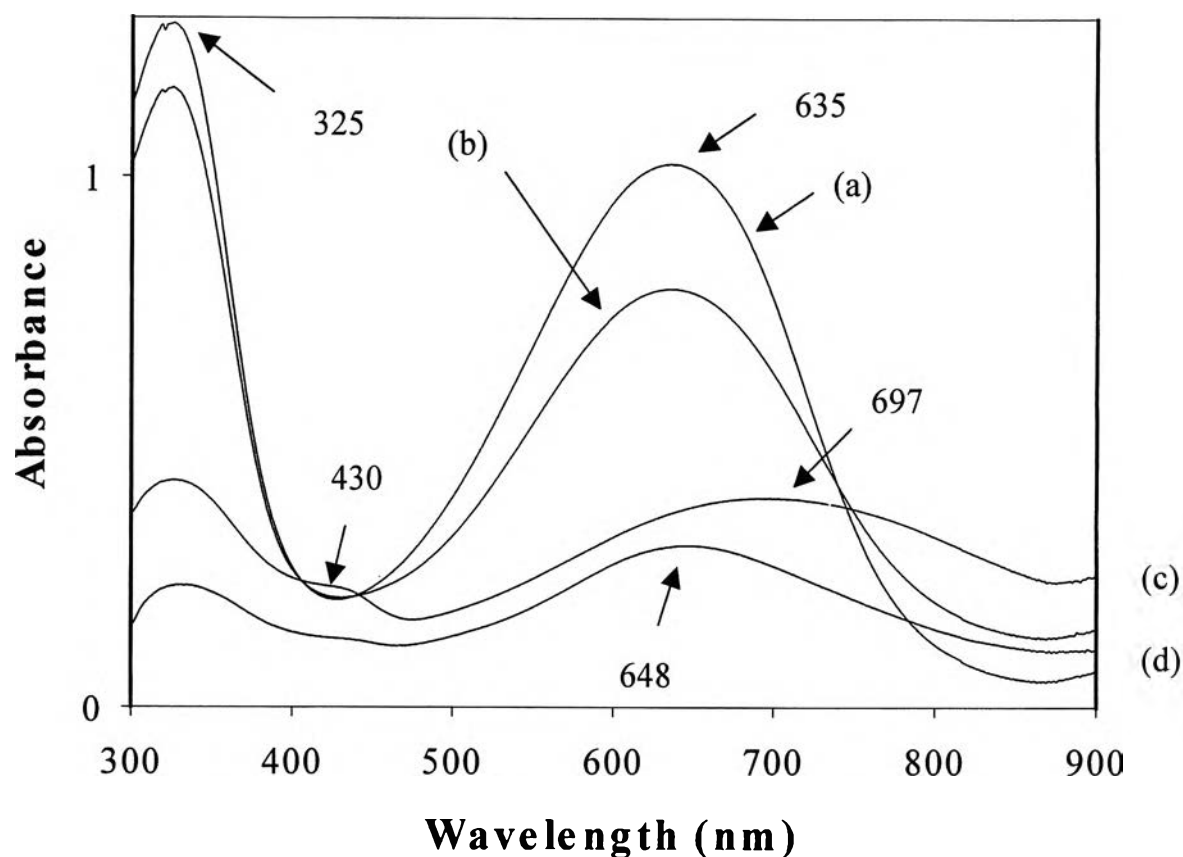
Figure 4.4 UV-Vis Spectra of PANI-H₂SO₄/HCOOH at N_{EB}/N_A of: (a) 1:4 ;
(b) 1: 40; (c) 1: 200; and (d) 1: 400.

In the theory electronic band structure of organic semiconductors, the
mobile discontinuities manifest themselves as mid-gap states (Blackwood and
Josowicz,1991). The diagram of the predicted electronic structures for a
conducting polymer in its neutral states containing polarons and bipolarons is
shown in Scheme 4.1. In the case of a *p*-type-doped conducting polymer the
polaron state contains one electron and the bipolaron state is completely
empty.
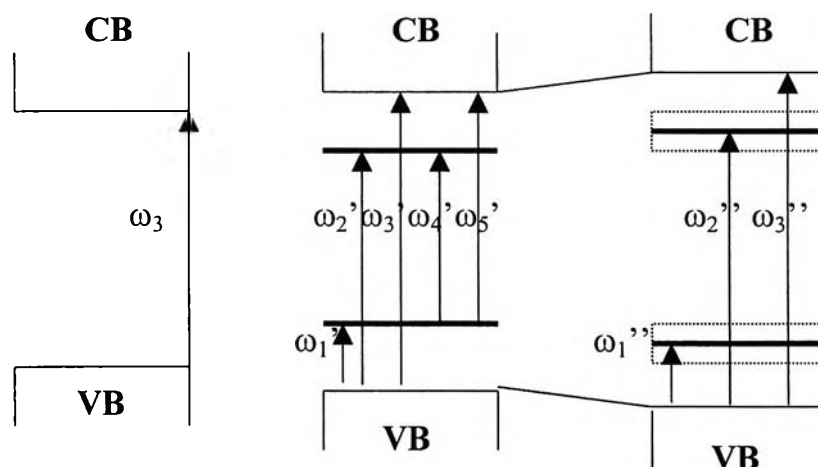
Scheme 4.1 Electronic structure of the bandgap of conducting polymers in their neutral, polaron (light doping) and bipolaron (heavy doping) states.

Scheme 4.1 shows the electronic transitions that might be expected to occur in p-type polypyrrole and p-polyphenylene under the radiation of ultraviolet or visible light. Kaufman et al, (1985) showed that the energy levels for the polaron and bipolaron mid-gap states are close enough to one another so, it is safe to assume that ω_1' $\approx \omega_1$'', ω_2' $\approx \omega_2$''. Since the formation of a polaron involves only the removal of one electron from the valence band it can also be assumed that $\omega_3 \approx \omega_3$'. However, it can also be shown that at high doping levels the bipolaron energy states can overlap into bands of their own thus causing ω_3'' to increase due to the fact that the bipolaron state originates from the valence and conduction band edges.

Since transition ω_1', ω_2' and ω_3' involve promoting electrons from the full valence band whereas ω_4' and ω_5' arise from only the half-filled polaron level, it may be expected that the three former transitions will dominate the polymer spectra. In a p-type conducting polymer the polaron and bipolarons can be considered as cation and dication species, respectively, and thus it can be visualized that a p-type polymer film could be reduced in the following ways:

$$\text{bipolaron} + e \longrightarrow \text{polaron} \tag{1}$$

$$\text{polaron} + e \longrightarrow \text{neutral} \tag{2}$$
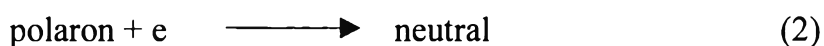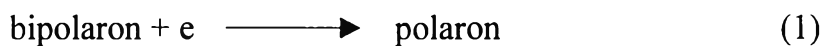
Likewise it could be oxidized as

$$\text{polaron} + e \longrightarrow \text{bipolaron} \tag{3}$$

$$\text{neutral} + e \longrightarrow \text{polaron} \tag{4}$$

The changes in the intensities of the transitions that occur if the conducting polymer undergoes one of the reactions 1-4 are expected to be:

reaction 1, ω_1 increases, ω_4 and ω_5 decrease, ω_2 and ω_3 unchanged;

reaction 2, ω_3 increases, ω_1 ,ω_2 ,ω_4 , and ω_5 decrease;

reaction 3, ω_1 decreases, ω_4 and ω_5 increase, ω_2 and ω_3 unchanged;

reaction 4, ω_3 decreases, ω_1, ω_2, ω_4 and ω_5 increase.

As a consequence of the above assignments, it is evident that if electron density is donated into the polymer chain there would always be an increase in the amount of light absorbed at wavelengths with energies less than that required for the transition ω_4 to occur (Blackwood and Josowicz, 1991).

According to UV-Vis result, dedoping process occurred in PANI-H_2SO_4/HCOOH. It can be explained in terms of an equilibrium equation. Protonation :
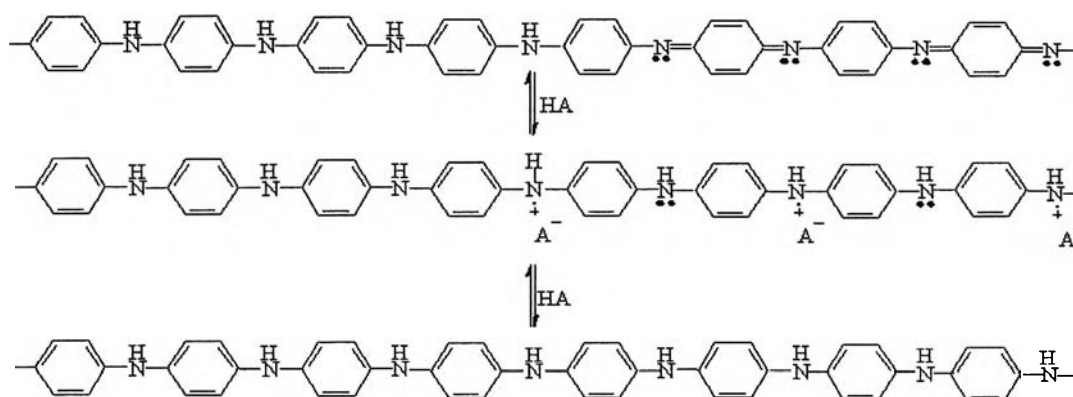
Scheme 4.2 The mechanism of dedoping process.

When the polymer chain attained the fully protonated state, there was no N imine site left in the polymer chain. As the amount of acid dopant was increased, the H^+ atom from the acid dopant drew back the counter ions which were attached to the protonated N imine sites. This resulted in the reoccurrence of unprotonated N imine sites. This caused a shift in the neutral peak of 697 nm to the peak of 648 nm.

Table 4.1 Assignments for UV-Visible spectra of undoped and doped polyanilines at aturated state.

Wavelength (nm)						Assignments	References
PANI	PANI-HCl/HBr*	PANI-HCl/MA*	PANI-H₂SO₄/HNO₃	PANI-H₂SO₄/HCOOH	PANI/CSA		
324 [325]	332	314	317	317	325	Transition of the EB benzene ring	Sertova *et al.*, 1998
	434	430	435	432	430 [425]	Changing of quinoid segments to the bipolaron state	Hunag *et al.*, 1993
633 [630]		650			635-697	The excitation of quinoid ring	Wan *et al.*, 1992
			763 [764]			The positive radical of the polaron state in the polyaniline salt	Pereira du silva *et al.*, 1993
	841	792		780 [780]		Localized polaron	Zheng *et al.*, 1992

Table 4.2 Assignments for UV-Visible spectra of doped polyaniline at various doping ratios

Wavelength (nm)						Assignments	References
N_A/N_{EB}	PANI-HCl/HBr*	PANI-HCl/MA*	PANI-H_2SO_4/HNO$_3$	PANI-H_2SO_4/HCOOH	PANI/CSA		
4	332 [325]	317	314	317	325	Transition of the EB benzene ring	Sertova et al., 1998
	440 [425]			440		Changing of quinoid segments to the bipolaron state	Hunag et al., 1993
		616	597		635 [630]	The excitation of quinoid ring	Wan et al., 1992
	821			787 [780]		Localized polaron	Zheng et al., 1992
40	350	314	317	320	325 [325]	Transition of the EB benzene ring	Sertova et al., 1998
	440	430		430 [425]		Changing of quinoid segments to the bipolaron state	Hunag et al., 1993

N_A/N_EB	Wavelength (nm)					Assignments	References
	PANI-HCl/HBr*	PANI-HCl/MA*	PANI-H₂SO₄/HNO₃	PANI-H₂SO₄/HCOOH	PANI/CSA		
		650			635 [630]	The excitation of quinoid ring	Wan *et al.*, 1992
	819	792	763	769 [780]		Localized polaron	Zheng *et al.*, 1992
200	351	289	309	285	325 [325]	Transition of the EB benzene ring	Sertova *et al.*, 1998
	440	435	430	435	435 [425]	Changing of quinoid segments to the bipolaron state	Hunag *et al.*, 1993
		655 [630]			697	The excitation of quinoid ring	Wan *et al.*, 1992
	770 [780]		773	790		Localized polaron	Zheng *et al.*, 1992
400	358	287	306	286	328 [325]	Transition of the EB benzene ring	Sertova *et al.*, 1998

N_A/N_{EB}	Wavelength (nm)					Assignments	References
	PANI-HCl/HBr*	PANI-HCl/MA*	PANI-H_2SO_4/HNO_3	PANI-H_2SO_4/HCOOH	PANI/CSA		
	440	440	435 [425]	432	432	Changing of quinoid segments to the bipolaron state	Hunag et al., 1993
		627 [630][			648	The excitation of quinoid ring	Wan et al., 1992
	744		794 [780]	717		Localized polaron	Zheng et al., 1992

* Data obtained from Sangswarng, 2001

4.1.2 FI-IR Spectroscopy.

This technique was used to confirm the structure of synthesized PANI. The FT-IR spectrum of polyaniline emeraldine base (EB) is shown in Figure 4.5
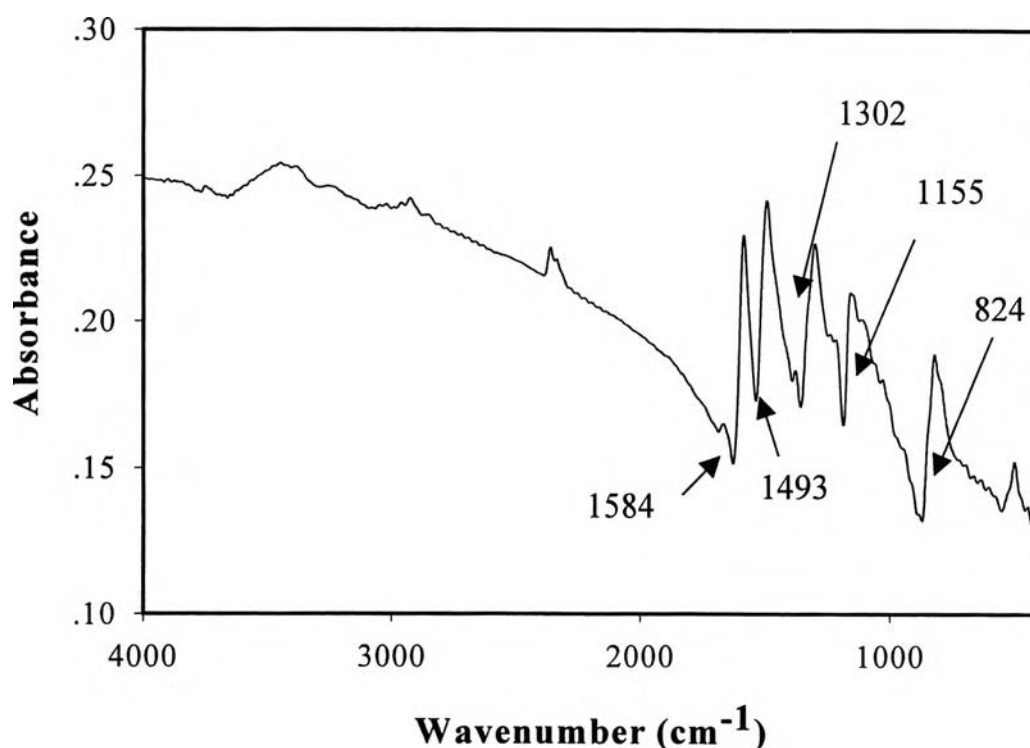

Figure 4.5 FT-IR spectrum of emeraldine base (EB).

The spectrum of emeraldine base shown 5 important absorption bands at 824, 1155, 1302, 1493 and 1584 cm^{-1}. These peaks are attributed to the out-of-plane bending vibration of C-H on *para*-disubstituted rings, characteristic vibrational mode of $N=\langle\ \rangle=N$, stretching vibration of C-H, stetching vibration of $N—\langle\ \rangle—N$ ring and stretching vibration of $N=\langle\ \rangle=N$ Rings, respectively (Zeng and Ko, 1998).

The spectrum of PANI-H$_2$SO$_4$/CSA, PANI-H$_2$SO$_4$/HNO$_3$ and PANI-H$_2$SO$_4$/HCOOH are shown in the Figure 4.6-4.8.
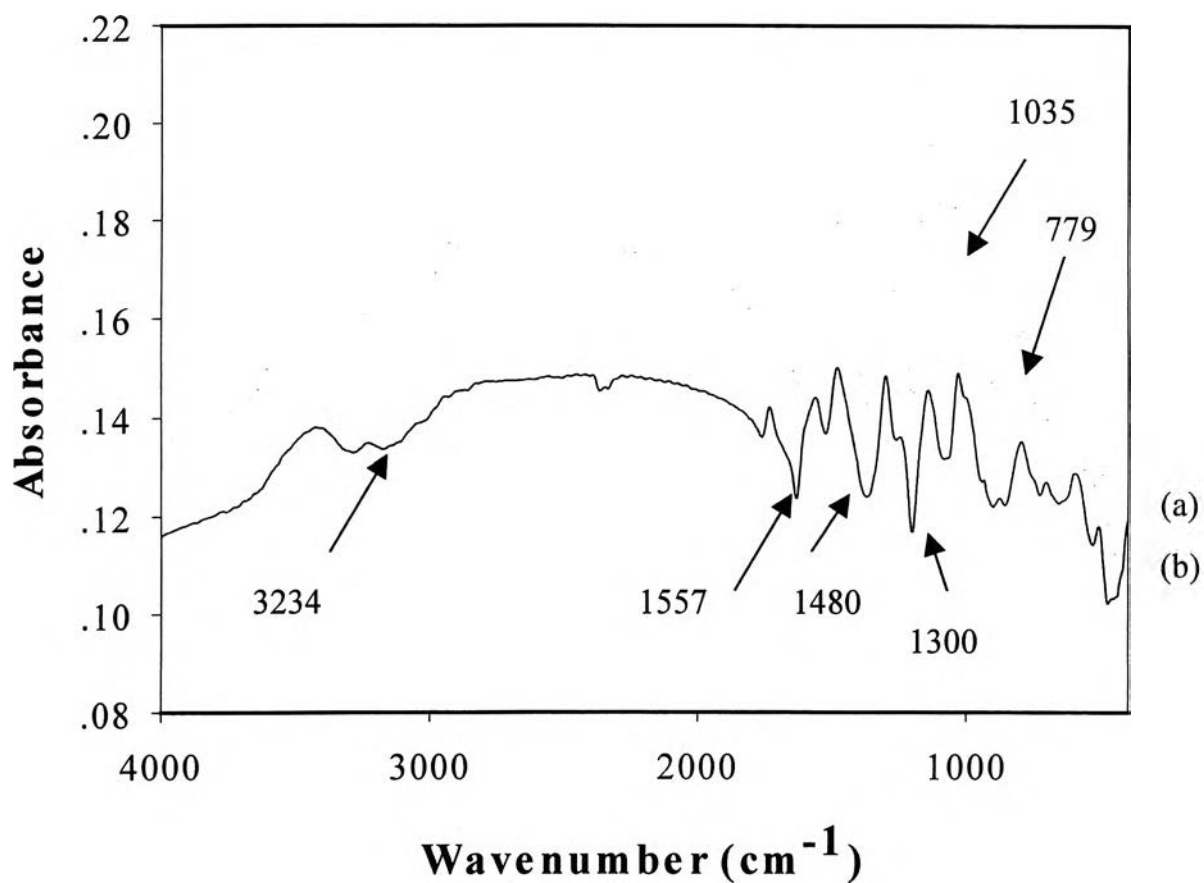
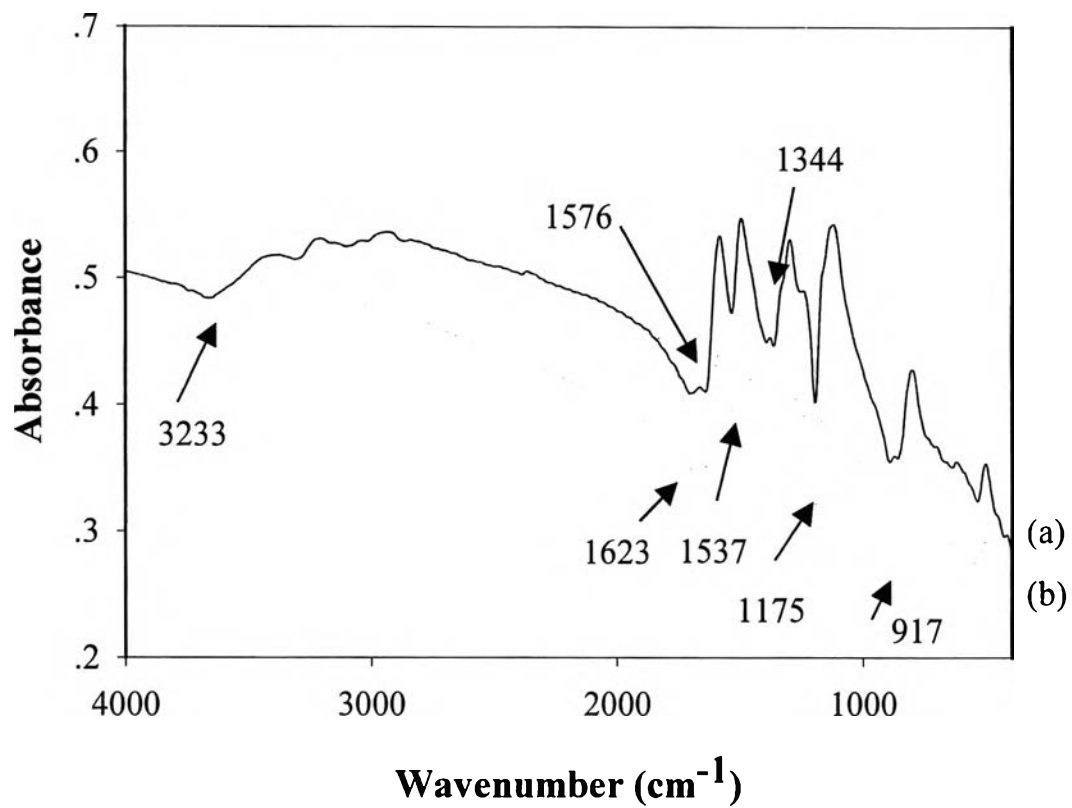**Figure 4.6** FT-IR spectra of PANI-H$_2$SO$_4$/CSA at N$_A$/N$_{EB}$ of : (a) 1:4 ; and (b) 1:40.

Figure 4.7 FT-IR spectra of PANI-H$_2$SO$_4$/HNO$_3$ at N$_{EB}$/N$_A$ of :(a) 1: 4 ;and (b) 1: 40.
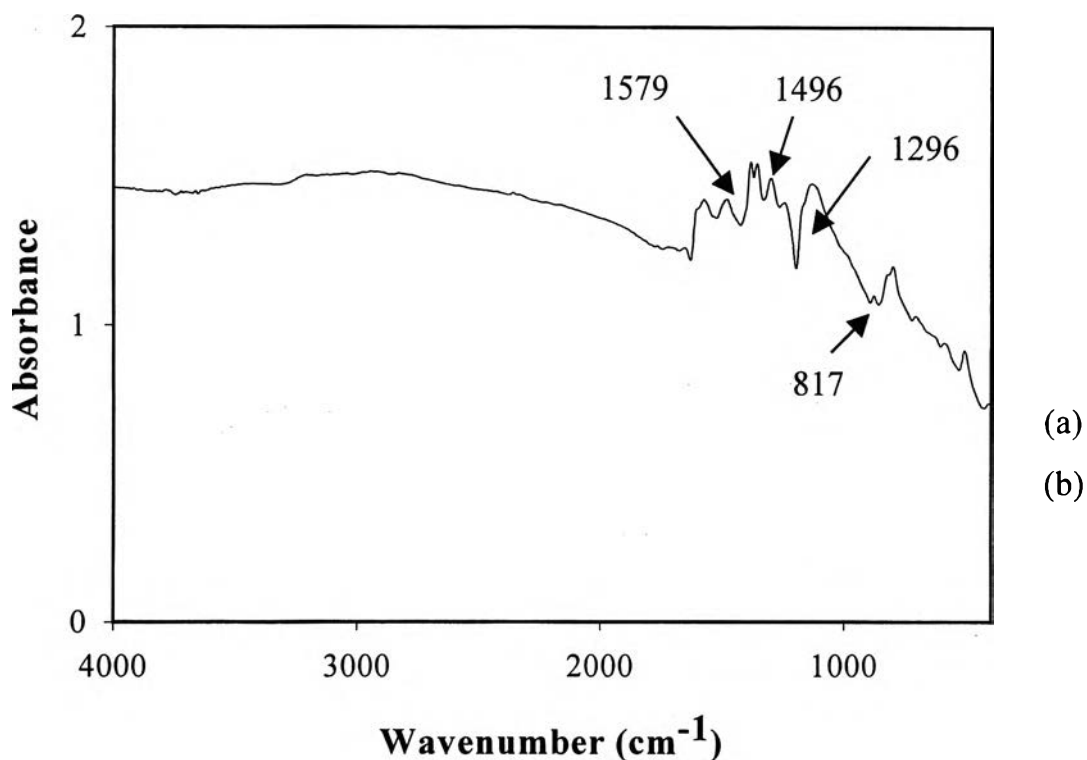
Figure 4.8 FT-IR spectra of PANI-H$_2$SO$_4$/HCOOH at N$_{EB}$/N$_A$ of :(a) 1: 4 ;and (b) 1: 40.

In the case of PANI-H$_2$SO$_4$/CSA, there was an additional absorption band at 1035 cm^{-1} represents the vibrational mode of sulfonic acid salt group (Aldrich Library of FT-IR Spectra, 1983). Consistent with PANI doped with CSA, PANI-H$_2$SO$_4$/HNO$_3$ had the an additional absorption band at 1623 cm^{-1}, indicated the vibrational mode of covalent nitrate, and the peaks at 1344 and 917 cm^{-1} identifing the vibrational mode of NO$_3^-$ (Wade, 1995).

The spectra of EB and doped-PANI have 5 important bands. The assignments of the bands are tabulated in the Table 4.3.

Table 4.3 Assignments for absorption bands of undoped and doped polyanilines.

Wavenumber (cm^{-1})						Assignments	References
PANI	PANI-HCl/HBr*	PANI-HCl/MA*	PANI-H$_2$SO$_4$/HNO$_3$	PANI-H$_2$SO$_4$/HCOOH	PANI-H$_2$SO$_4$/CSA		
3242± 3	3377± 5	3393± 1	3247± 3 [3100-3500]	3230± 3	3234± 2	NH stretching	Kang *et al.*(1998)
		1705± 3			1732± 3 [1741]	Stretching of C=O group of acid	The Aldrich library of FT-IR Spectra
			1623± 2 [1600-1650]			Vibrational mode of covalent nitrate	Wade *et al.*, (1995)
1584± 2	1580± 6	1556± 3	1576± 1	1579± 5 [1595]	1557± 6	C=N stretching of quinoid ring	Milton and Monkman *et al.*, (1993)

Wavenumber (cm^{-1})						Assignments	References
PANI	PANI-HCl/HBr*	PANI-HCl/MA*	PANI-H$_2$SO$_4$/HNO$_3$	PANI-H$_2$SO$_4$/HCOOH	PANI-H$_2$SO$_4$/CSA		
1493± 2	1496± 5	1496± 5	1537± 2	1496± 2 [1498]	1480± 1	Stretching of benzenoid ring	Zeng and Ko ,(1998)
			1344 ± 2 [1360-1430]			Vibrational mode of NO$_3^-$	Wade et al., (1995)
1297± 4	1292± 3	1303± 4	1317± 1	1296± 2 [1306]	1300± 2	C-N stretching of benzenoid ring	Show-An Chen et al., (1995)
		1223± 1	1228± 3 [1230]			C-N stretching through C-N-C angle	Levon et al., (1995)
1155± 5			1175 ± 4 [1165]			Broken symmetry mode of quinoid structure	Chan et al., (1994)

Wavenumber (cm^{-1})						Assignments	References
PANI	PANI-HCl/HBr*	PANI-HCl/MA*	PANI-H$_2$SO$_4$/HNO$_3$	PANI-H$_2$SO$_4$/HCOOH	PANI-H$_2$SO$_4$/CSA		
	1146± 2 [1140]			1129± 3	1145± 7	A mode of Q=N$^+$H-B or B-NH-B	Morales et al., (1977)
					1035± 6 [1059]	Sulfonic acid salt group	The Aldrich library of FT-IR Spectra
			917± 1 [800-860]			Vibrational mode of NO$_3^-$	Wade et al., (1995)
	878± 1 [850-910]	866± 2				CH out of plane bending of 1,2,4 ring	Zeng and Ko (1998)
824± 3			836± 1 [825]	817± 1		Out of plane bending of 1,4-ring	Milton and Monkman (1993)

Wavenumber (cm^{-1})						Assignments	References
PANI	PANI-HCl/HBr*	PANI-HCl/MA*	PANI-H$_2$SO$_4$/HNO$_3$	PANI-H$_2$SO$_4$/HCOOH	PANI-H$_2$SO$_4$/CSA		
			764 ± 4 [740]		779± 5	C-H out of plane bending of 1,2-ring	Kang *et al.*(1998)

- N$_A$/N$_{EB}$ = 4, 40, 200, 400

* Data obtained from Sangswarng, 2001

47

4.1.3 Thermal Gravity Analysis (TGA).

The thermal stability properties of PANI were observed by using TGA technique. TGA chromatogram of emeraldine base (EB) powder measured under N_2 atm is illustrated in Figure 4.9. It shows a typically three step weight loss. First, the loss of methanol and THF as the residual solvents in the synthesis process occurred about 40-60 °C. Secondly, the loss of water molecule occurred about 100°C. The third loss may be assigned to the loss of low molecular-weight oligomer. TGA did not show a significant weight loss until 510°C, where PANI chains began to decompose (Li and Wan, 1999).
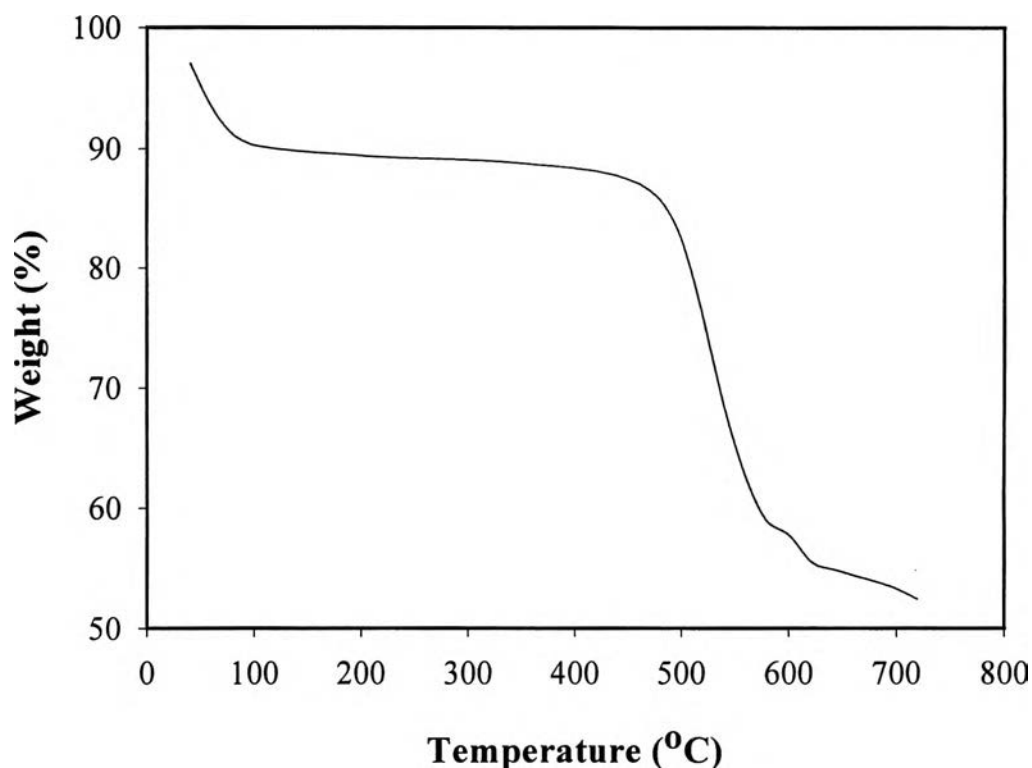

Figure 4.9 TGA chromatogram of emeraldine base (EB).

The chromatograms of doped-PANI are shown in Figure 4.10-4.12; they have an additional 1 stage weight loss. This was due to the loss of dopant molecule. The assignments are listed in Table 4.4.
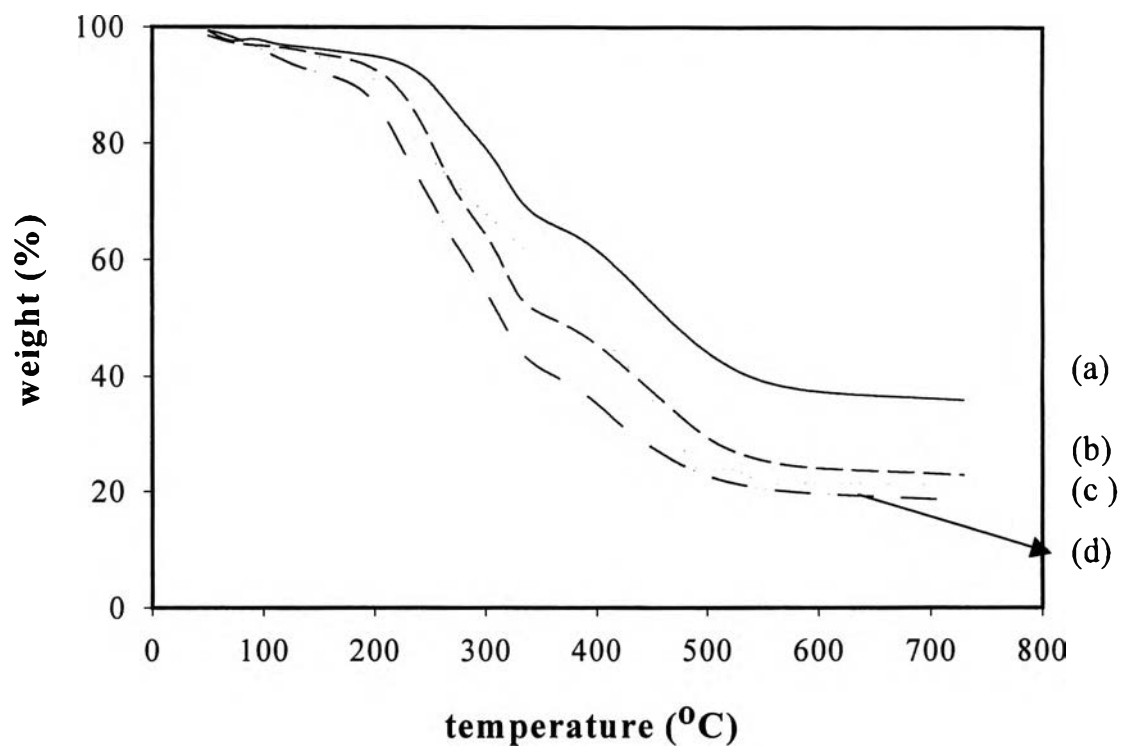

Figure 4.10 TGA chromatograms of PANI-H_2SO_4/CSA at N_{EB}/N_A of : (a) 1:4 ;(b) 1: 40; (c) 1: 200 ;and (d) 1: 400.
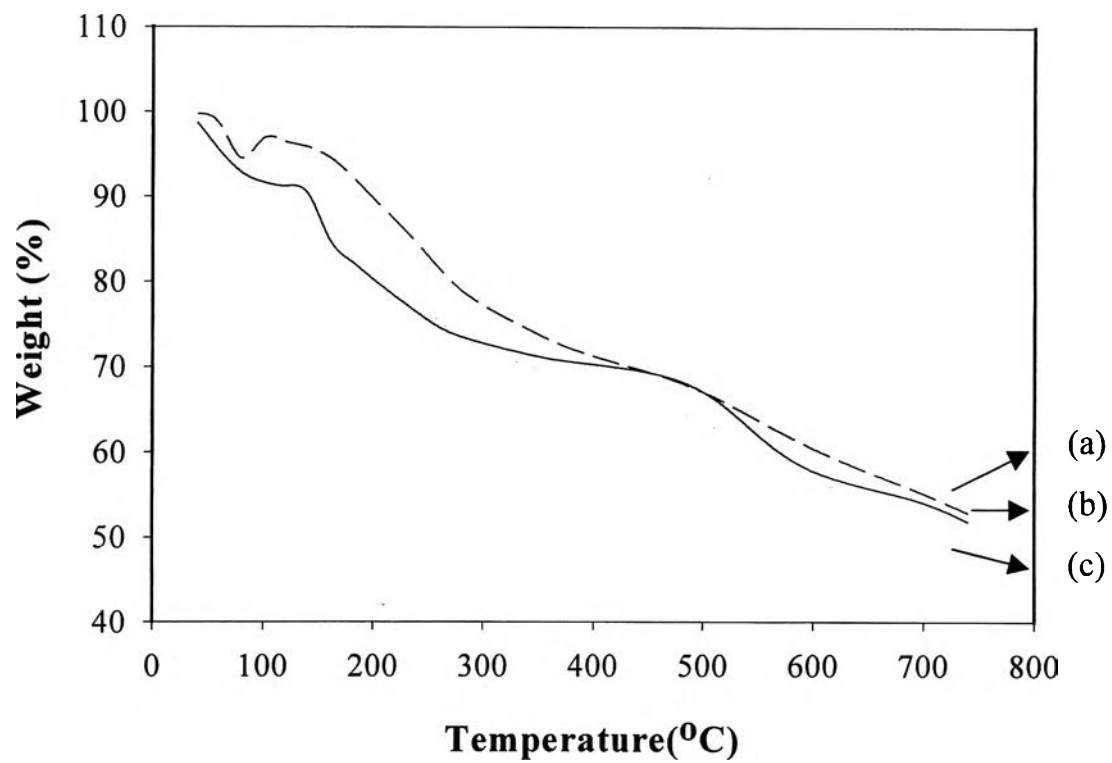
Figure 4.11 TGA chromatograms of PANI-H$_2$SO$_4$/HNO$_3$ at N$_{EB}$/N$_A$ of : (a) 1: 4; (b) 1: 40 ;and (c) 1: 200.
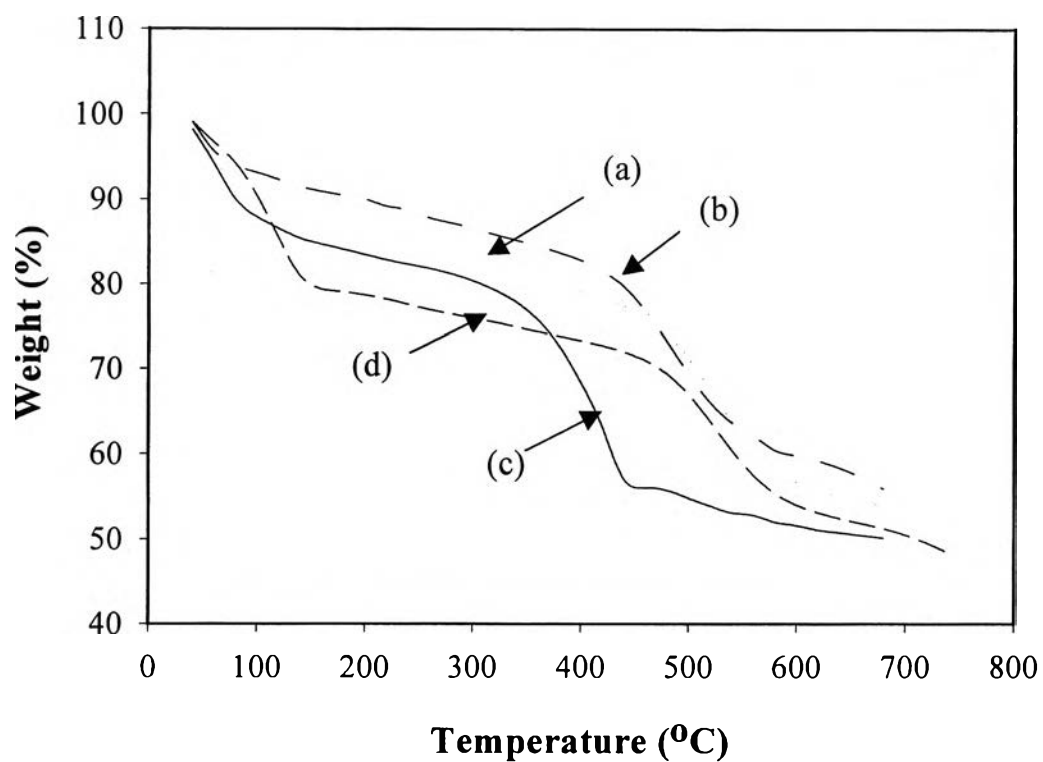
Figure 4.12 TGA chromatograms of PANI-H_2SO_4/HCOOH at N_{EB}/N_A of :
(a) 1: 4; (b) 1: 40; (c) 1: 200 ;and (d) 1: 400.

Table 4.4 Assignments for TGA thermogram of undoped and doped polyaniline.

Temperature (°C)						Assignments	References
PANI	PANI-HCl/HBr*	PANI-HCl/MA*	PANI-H$_2$SO$_4$/HNO$_3$	PANI-H$_2$SO$_4$/HCOOH	PANI/CSA		
39±5	48±8	44±6	55±8	49±14	53±10	The loss of solvent molecules (THF and Methanol)	Li et al., 1999
106±6 [110]	75±6	128±7	97±11	106±7	119±28	The loss of water molecule	Palaniappan et al., 1994
-	218±31	198±20	116±9 [110-275]	245±15	288±18	The loss of acid molecule as volatile gas	Palaniappan et al., 1994
522±19 [500]	557±28	521±4	505±25	504±16	478±12	Degradation of polymer backbone	Li et al., 1999

* Data obtained from Sangswarng, 2001

4.1.4 X-ray Diffractometry (XRD).

A typical x-ray diffraction pattern of polyaniline emeraldine base (EB) is shown in Figure 4.13.   Its pattern consists only of a broad band at $2\theta = 25°$, which can be associated with X-ray diffraction of amorphous region in the sample (Pouget *et al.*, 1991).
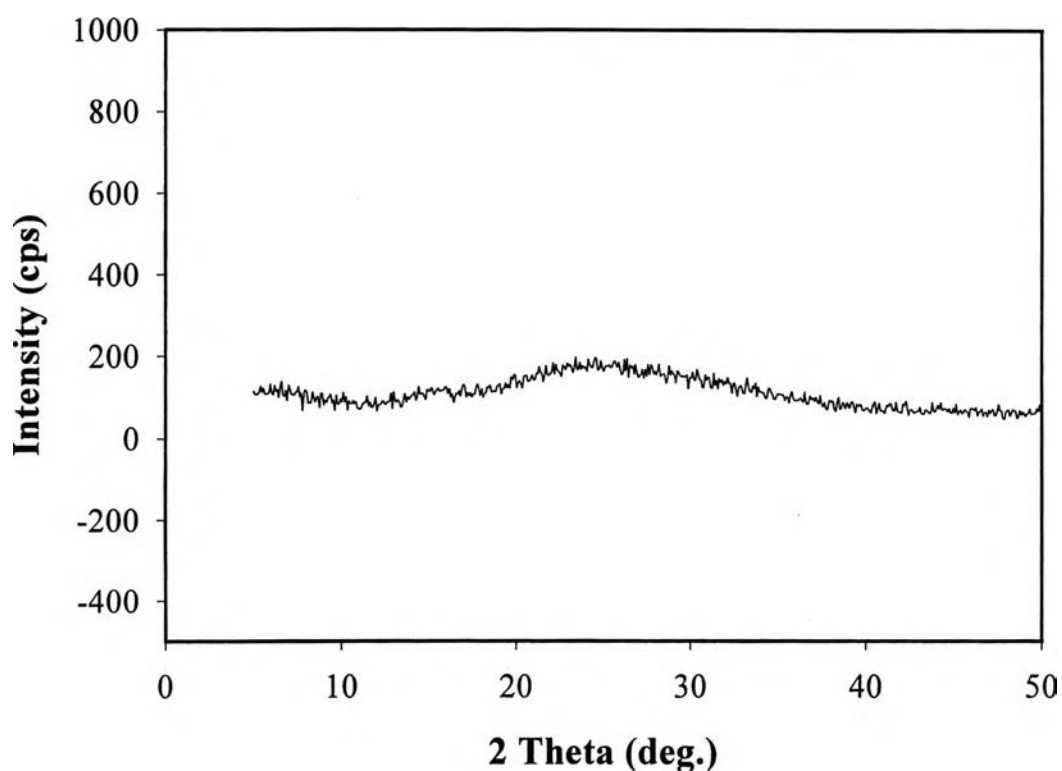

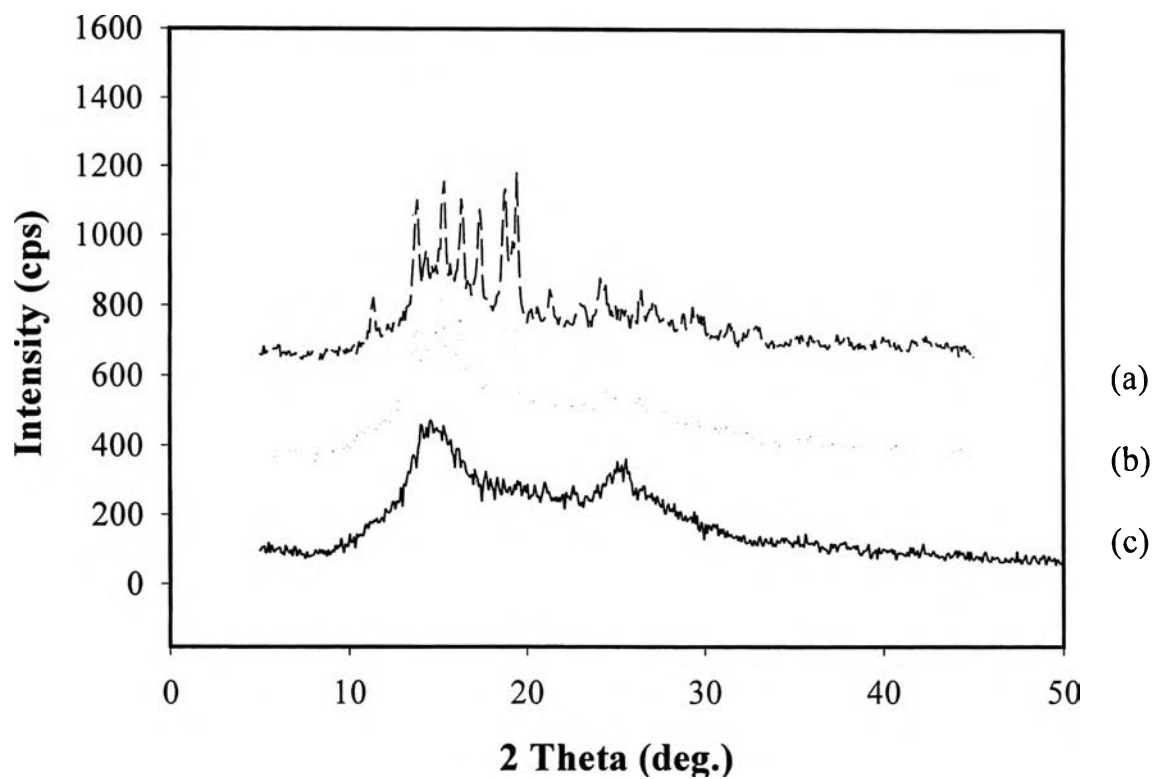**Figure 4.13** The XRD pattern of emeraldine base (EB).

Figure 4.14 XRD patterns of PANI-H_2SO_4/CSA at N_{EB}/N_A of :(a) 1:40; (b) 1: 200 ;and (c) 1: 625.
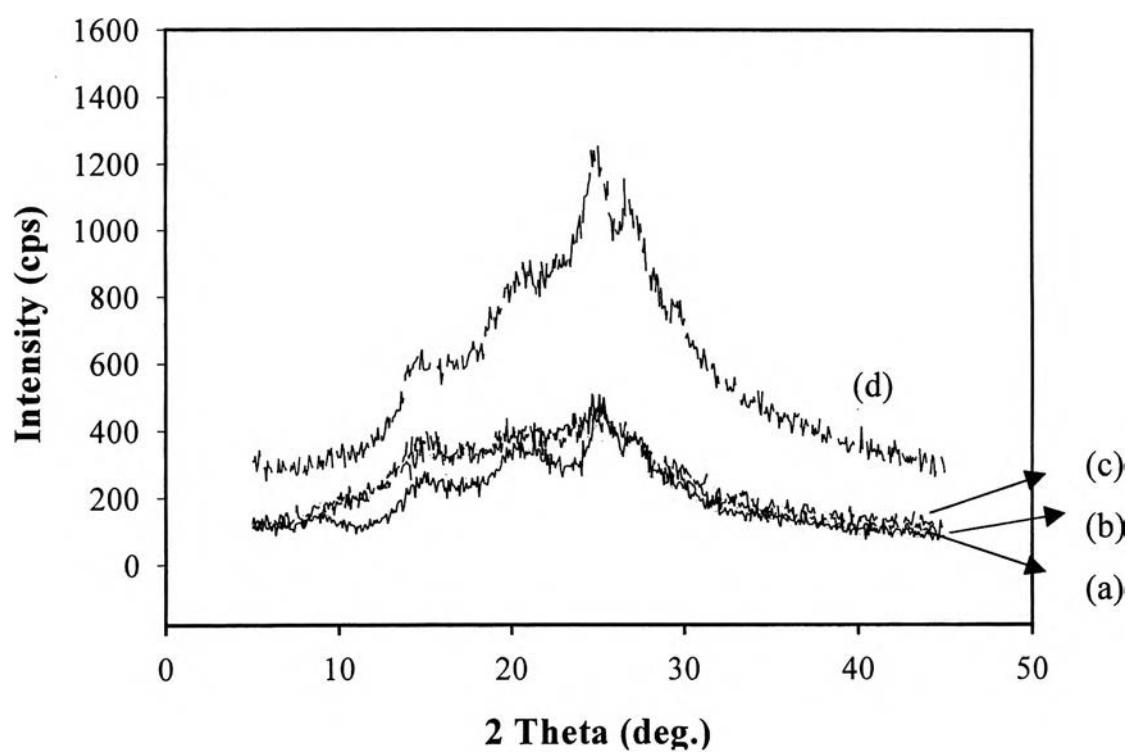
Figure 4.15 XRD patterns of PANI-H_2SO_4/HNO_3 at N_{EB}/N_A of: (a) 1: 4 ;
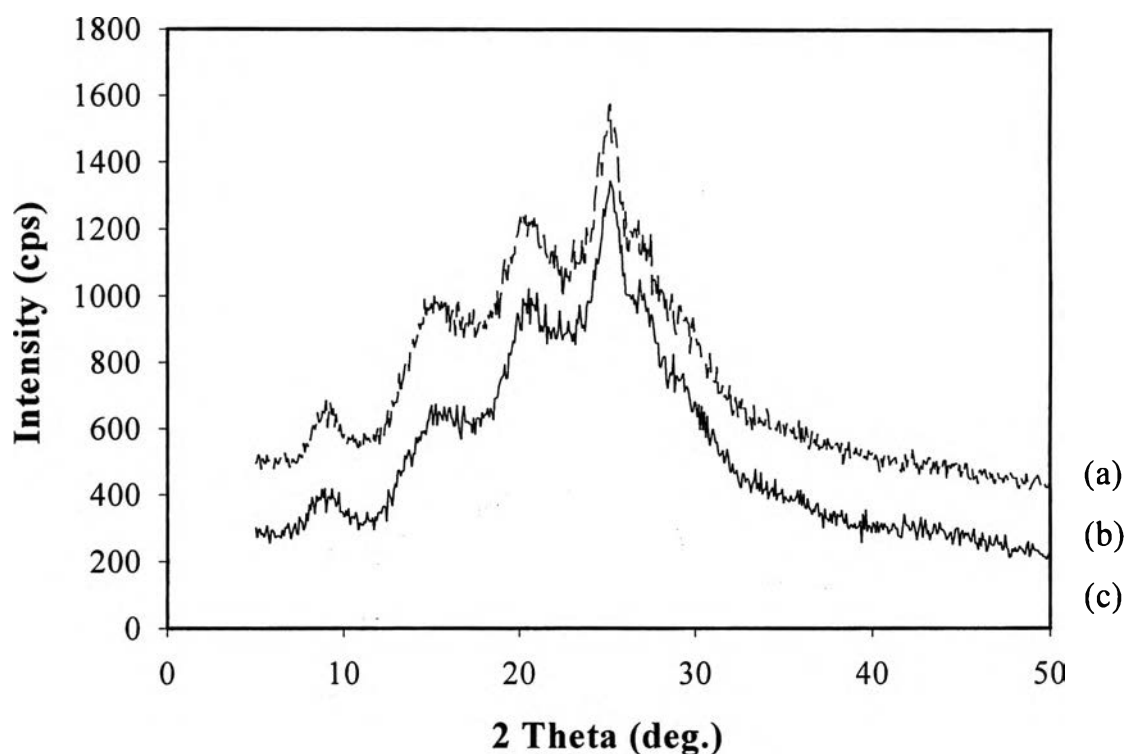(b) 1:30 ;(c) 1:40; and (d) 1:200.

Figure 4.16 XRD pattern of PANI-H_2SO_4/HCOOH at N_{EB}/N_A of :(a)1:200 ; (b) 1: 400 ;and (c) 1: 625.

Figure 4.14, 4.15 and 4.16 show XRD patterns of PANI-H_2SO_4/CSA, PANI-H_2SO_4/HNO_3 and PANI-H_2SO_4/HCOOH, respectively. The patterns obtained indicate that the degree of crystallinity increases with N_{EB}/N_A. This occurred as the amount of positive charges on the polymer backbone increased at higher doping molar ratios. The repulsive effect of these positive charges caused the polymer chains to extend toward a crystalline structure. The main characteristic peak at $2\theta \approx 11°$ (d spacing ≈ 8.04 A°) indicates the distance between the polymer chains, and it can correspond to the (001) reflection (Pouget, 1991).

Table 4.5 The value of 2theta and d-value of undoped and doped polyaniline.

Sample	N_A/N_{EB}	2Theta (deg.)	d-value (A°)
PANI-HCl*	-	19.40, 19.53	4.57, 4.59
		36.60, 36.63	2.45, 2.50
PANI-HCl/HBr*	1293	9.44, 9.45	9.36, 9.40
		15.10, 15.21	5.86, 5.89
		20.52, 20.54	4.32, 4.35
		24.98, 25.02	3.56, 3.59
		26.92, 26.96	3.31, 3.39
		29.78, 29.82	2.99, 3.04
	400	20.44, 20.48	4.34, 4.39
		25.02, 25.03	3.56, 3.58
		27.08, 27.12	3.29, 3.33
	200	15.32, 15.22	5.78, 5.82
		20.65, 21.00	4.31, 4.23
		25.10, 25.16	3.54, 3.54
		27.10, 27.36	3.29, 3.26
	160	15.38, 15.88	5.76, 5.58
		21.04, 21.20	4.22, 4.19
		25.00, 25.02	3.56, 3.56
		27.14, 26.88	3.28, 3.31
	80	15.20, 15.22	5.82, 5.84
		20.68, 20.71	4.29, 4.29
		25.02, 25.04	3.56, 3.57
	4	9.40, 9.43	9.40, 9.42
		14.88, 14.91	5.95, 5.96
		20.68, 20.73	4.29, 4.31

Sample	N_A/N_{EB}	2Theta (deg.)	d-value (A°)
		25.22, 25.26	3.53, 3.55
		30.62, 30.65	2.92, 2.96
PANI-HCl/CSA*	160	11.48, 11.36	7.70, 7.78
		13.94, 13.82	6.35, 6.40
		14.40, 14.36	6.15, 6.16
		15.48, 15.32	5.72, 5.78
		16.48, 16.32	5.37, 5.42
		17.52, 17.40	5.05, 5.09
		18.90, 18.78	4.69, 472
		19.58, 19.44	4.53, 4.56
		21.42, 21.32	4.14, 4.16
		24.24, 24.02	3.67, 3.70
	40	15.50, 15.24, 15.00	5.71, 5.81, 5.70
		16.52, 16.24, 16.62	5.36, 5.45, 5.33
		17.52, 17.30, 17.28	5.06, 5.12, 5.13
		18.94, 18.68, 18.26	4.68, 4.45, 4.85
		21.50, 21.22, 21.12	4.13, 4.18, 4.22
		24.30, 24.80, 24.28	3.66, 3.89, 3.66
	20	15.04, 15.05	5.89, 5.93
		25.18, 25.20	3.53, 3.54
	4	14.66, 14.84	6.04, 5.96
		25.20, 25.06	3.53, 3.55
	2	14.80, 14.83	5.98, 6.01
		25.20, 25.22	3.53, 3.54
PANI-HCl/MA*	1293	17.48, 17.52, 17.50	5.07, 5.06, 5.06
		22.38, 22.42, 22.42	3.97, 3.96, 3.96
		25.08, 25.10, 25.20	3.55, 3.54, 3.53

Sample	N_A/N_{EB}	2Theta (deg.)	d-value (A°)
		27.98, 28.04, 2802	3.19, 3.18, 3.18
	800	9.08, 9.12	9.73, 9.69
		15.14, 15.46	5.85, 5.73
		20.64, 20.10	4.29, 4.11
		24.72, 25.24	3.59, 3.53
	400	15.82, 15.85	5.59, 5.61
		17.56, 17.60	5.05, 5.08
		19.94, 19.95	4.45, 4.46
		22.40, 22.41	3.97, 3.99
		25.06, 25.08	3.55, 3.58
		26.92, 26.93	3.31, 3.32
	200	15.58, 15.74, 15.86	5.68, 5.63, 5.58
		17.76, 17.50, 17.54	4.99, 5.06, 5.05
		20.24, 21.00, 20.26	4.22, 4.38, 4.35
		22.36, 22.42, 22.48	3.96, 3.97, 3.95
		25.18, 25.26, 25.06	3.53, 3.52, 3.50
		28.02, 28.86, 28.73	3.18, 3.09, 3.12
	40	15.00, 15.02	5.90, 5.91
		20.18, 20.22	4.39, 4.39
		25.20, 25.23	3.53, 3.55
	20	15.50, 15.36	5.71, 5.76
		20.36, 20.18	4.36, 4.39
		25.04, 25.04	3.55, 3.55
PANI-H_2SO_4/HNO_3	200	9.36, 9.39	9.44, 9.45
		14.54, 14.56	6.08, 6.10
		20.02, 20.03	4.43, 4.48
		22.62, 22.65	3.93, 3.96

Sample	N_A/N_{EB}	2Theta (deg.)	d-value (A°)
		24.88, 24.89	3.58, 3.60
		26.98, 26.70	3.30, 3.33
	200	11.38, 11.41	7.77, 7.78
		14.36, 14.37	6.16, 6.18
		19.48, 19.50	4.64, 4.67
		21.38, 21.39	4.15, 4.18
		24.02,24.03	3.70, 3.72
		25.34, 25.36	3.51, 3.53
	40	11.32, 11.35	7.81, 7.83
		13.76, 13.79	6.43, 6.46
		15.28, 15.31	5.79, 5.82
		16.28, 16.32	5.44, 5.46
		17.28, 17.32	5.13, 5.16
		18.68, 18.71	4.75, 4.78
		19.36, 19.37	4.58, 4.59
	30	15.12, 15.15	5.85, 5.85
		250.4, 25.08	3.55, 3.57
	10	15.12, 15.16	5.85, 5.86
		25.18, 25.22	3.53, 3.53
	4	15.06, 14.66	5.88, 6.04
		25.30, 25.20	3.52, 3.53
PANI-H₂SO₄/CSA	1293	15.72, 15.75	5.82, 5.84
		20.18, 20.23	4.39, 4.40
		25.08, 25.10	3.55, 3.58
		27.10, 27.11	3.29, 3.33
		29.38, 29.42	3.04, 3.04
	400	15.28, 15.28	5.79, 5.80

Sample	N_A/N_{EB}	2Theta (deg.)	d-value (A°)
		20.16, 20.18	4.40, 4.42
		24.62, 24.68	3.61, 3.63
		26.34, 26.36	3.38, 3.39
		26.46, 26.48	3.37, 3.38
	200	15.02, 15.05	5.89, 5.92
		20.58, 20.59	4.31, 4.35
		25.08, 25.10	3.55, 3.57
		26.92, 26.95	3.31, 3.32
		29.72, 29.73	3.00, 3.02
	160	11.50, 11.38	7.69, 7.77
		15.46, 15.36	5.73, 5.76
		18.90, 18.78	4.69, 4.72
		19.60, 19.48	4.53, 4.55
	40	14.92, 15.26, 15.28	5.93, 5.80, 5.79
		19.40, 20.18, 19.36	4.57, 4.39, 4.58
PANI-H₂SO₄/HCOOH	400	9.46, 9.51	9.34, 9.35
		15.28, 15.29	5.79, 5.79
		20.16, 20.19	4.40, 4.42
		24.62, 24.64	3.61, 3.61
	200	15.44, 15.02	5.73, 5.89
		24.50, 25.08	3.63, 3.55
	50	15.78, 15.79	5.61, 5.62
		24.30, 24.34	3.66, 3.68
	4	15.00, 15.03	5.90, 5.92
		20.20, 20.22	4.39, 4.40
		24.96, 24.98	3.56, 3.58
		29.30, 29.33	3.05, 3.06

Table 4.6 Comparison of experimental 2theta obtained from undoped and doped polyaniline with the results of model calculations.

2theta (deg.)	d-value (A°)	Reflection	References
9.44	9.3610	(010)	
15.10	5.8625	(100)	
20.52	4.3246	(040)	Winokur *et al.*,
24.98	3.5617	(110)	(1998)
26.92	3.3092	(012)	
29.78	2.9976	(112)	

Table 4.7 The assignment of XRD pattern of HCl-doped polyaniline films atCa/Cp = 10:1 (Pouget *et al*., 1991)

2θ (deg.)	d-spacing, (A°) (experiment)	d-spacing, (A°) (reference)	*(hkl)*	Assignments
8.7	10.16	9.57	(001)	Distance between polymer chains
15.22	5.81	5.94	(010)	Cl-N distance
20.18	4.40	4.26	(100)	-
25.08	3.55	3.51	{(110)}	-
27.1	3.29	3.28	{(111)}	-
29.38	3.04	2.98	(020)	-

(hkl) means the miller indices of planes

{*(hkl)*}means a set of reflections with permutation of the sign of the Miller indices

•Data obtained from Sangswarng, 2000

4.1.5 Scanning Electron Microscope (SEM).

SEM technique was used to study the morphology of polyaniline powder after doping with different acid dopants and at different doping levels. It was expected that these two parameters influence the morphology of polyaniline and hence electrical conductivity of polyaniline. SEM micrographs (magnification 3500 times) of undoped polyaniline, PANI-H_2SO_4/CSA, PANI-H_2SO_4/HNO_3 PANI-H_2SO_4/HCOOH are shown in Figures 4.17 , 4.18, 4.19 and 4.20, respectively. The morphology of PANI-H_2SO_4/CSA changed from globular to fibrillar with increasing of N_{EB}/N_A. It can be explained by the mechanism as shown in Scheme 4.3. At lower N_{EB}/N_A, the backbone was partially protonated by acid dopant. So, it still had some intramolcular H-bonding. This resulted in the appearance of the globular morphology. As N_{EB}/N_A was increased, the degree of protonation was increased, resulting in the expansion of the polymer chain. This can be explained in terms of the increase in the intermolecular H-bonding and the decrease in intramolecular H-bonding.
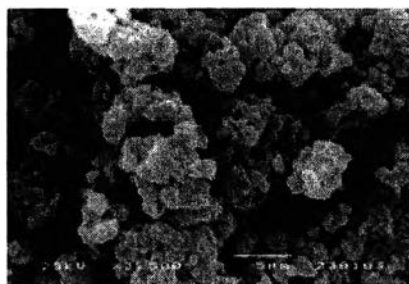
Figure 4.17 SEM micrographs of emeraldine base (EB).
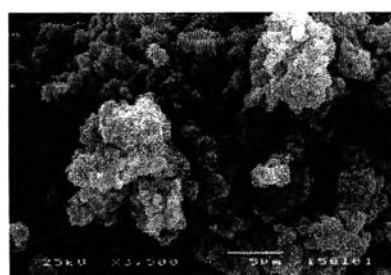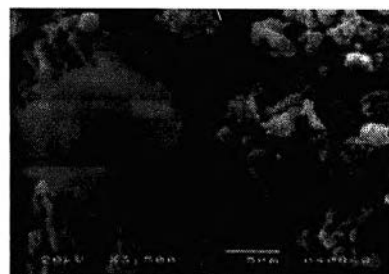

(a)   (b)
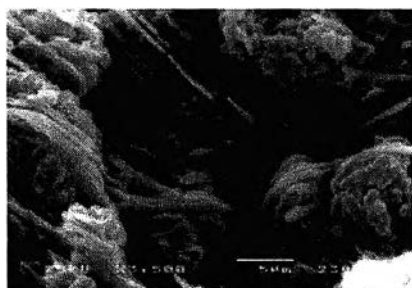
(c)

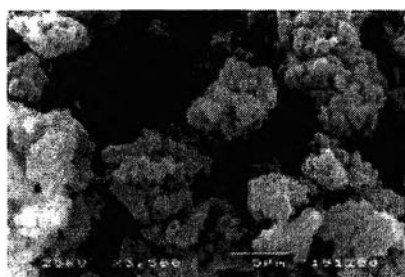**Figure 4.18** SEM micrographs of PANI-H_2SO_4 /CSA at N_{EB}/N_A of :(a) 1:4 ; (b) 1:40 ;and (c) 1:160.
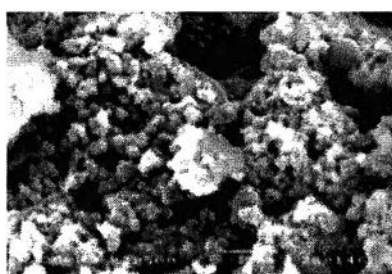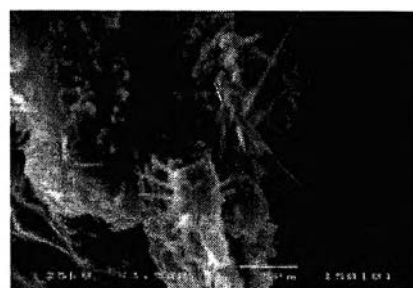

(a)

(b)

Figure 4.19 SEM micrographs of PANI-H_2SO_4/HNO_3 at N_{EB}/N_A of : (a) 1:4 ;and (b) 1:200.
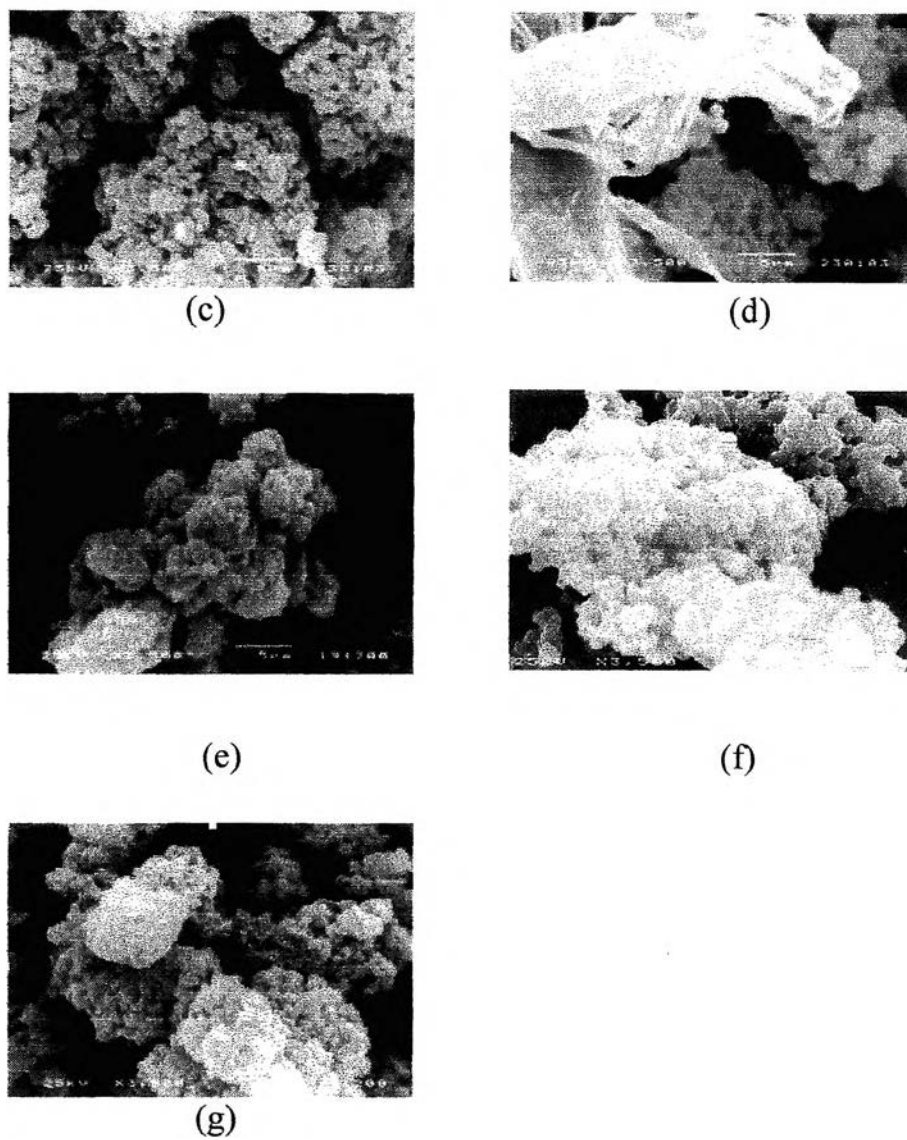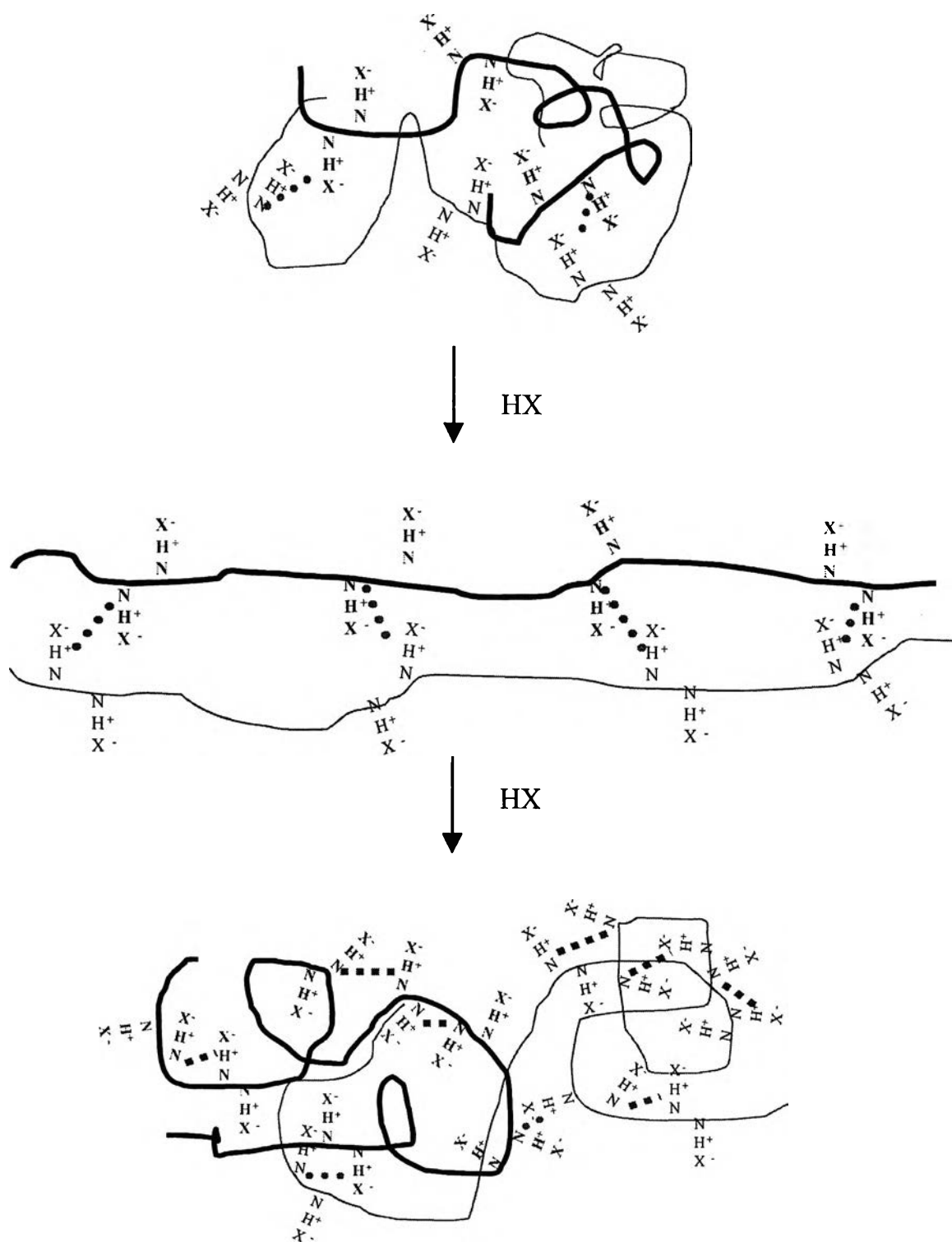

(a)

(b)

Figure 4.20 SEM micrographs of PANI-H_2SO_4/HCOOH at N_{EB}/N_A of :
(a) 1:4 ;(b) 1:40 ;(c) 1: 50 ;(d) 1:180 ;(e) 1:200 ;(f) 1: 400 ;and (g) 1: 625.

Scheme 4.3 The proposed mechanism of inter and intrachain H-bonding when N_{EB}/N_A is increased.

4.2   Electrical Conductivity

4.2.1   Effect of Dopant Types and Acid/Polymer Mole ratios (N_A/N_{EB}) on the Specific Conductivity.

In this research, CSA, HNO_3, and HCOOH were used as acid dopants. The conductivity of polyaniline pellet was measured by using the four-point probe under atmospheric pressure, $60 \pm 5\%$ relative humidity and $28 \pm 2°C$.

The polyaniline powder was kept in a desiccator before being fabricated into a pellet shape by using a hydraulic press under the pressure of 39.2 N/cm^2. The pellet thickness was measured by using a thickness gauge. Then, the polyaniline pellets were heated at $50°C$ for 2 days and kept in the desiccator before conductivity measurement in order to get rid of moisture.

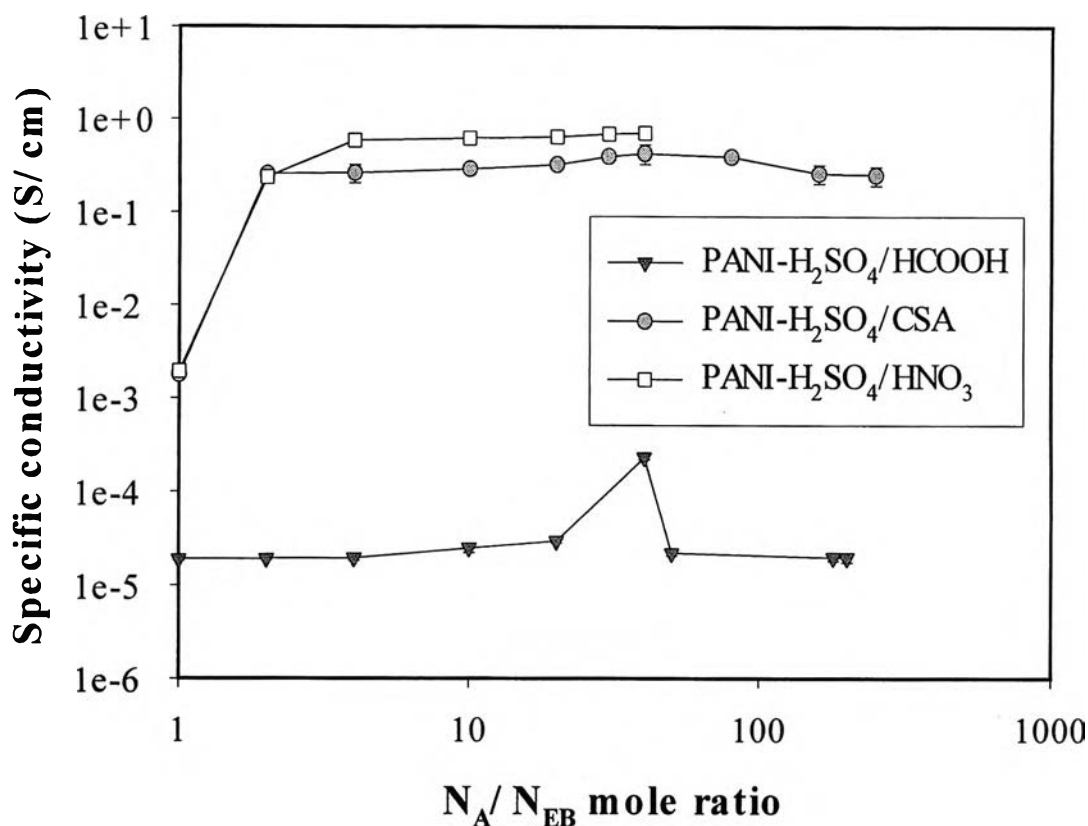The specific conductivity of doped PANI in air is shown in the Figure 4.21.
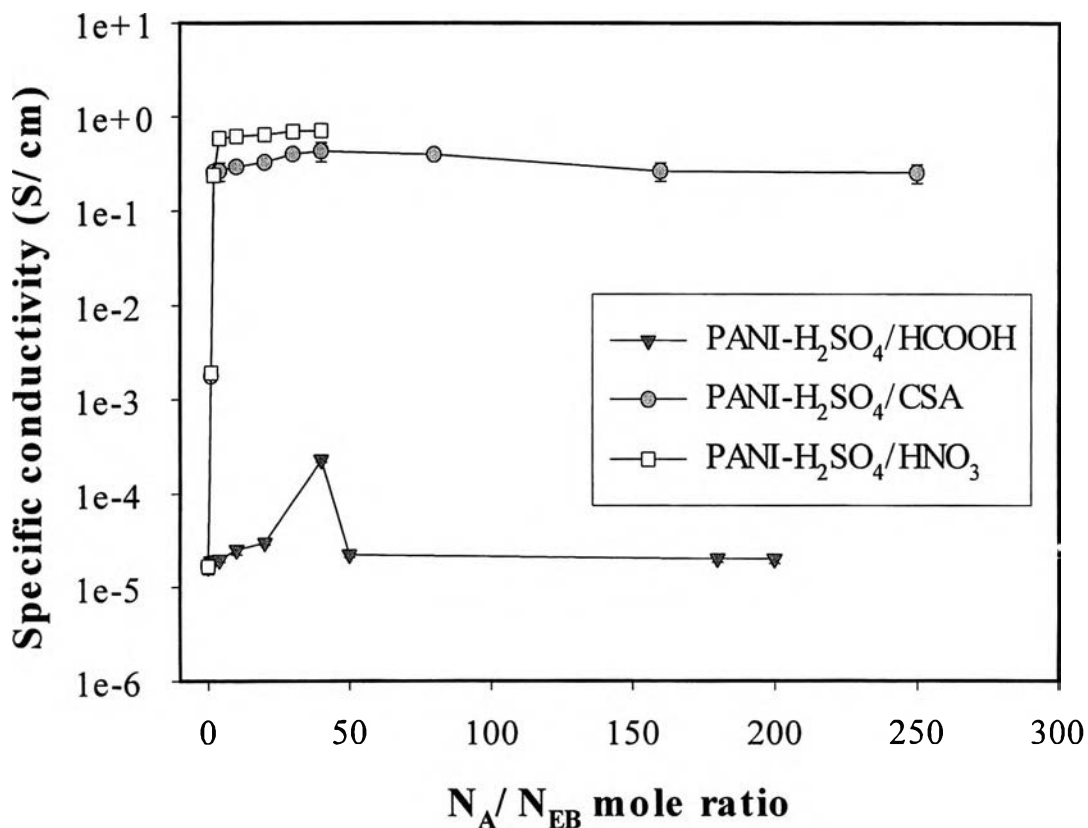
Figure 4.21 The specific conductivity of PANI-H_2SO_4/CSA, PANI-H_2SO_4/HNO_3, PANI-H_2SO_4/HCOOH in air under the condition of 1 atm, 60±5% relative humidity and 28± 2°C.

Specific conductivity of doped PANI dramatically increases with N_{EB}/N_A. In the case of PANI-H_2SO_4/CSA and PANI-H_2SO_4/HCOOH, the specific conductivity achieves the maximum values at N_{EB}/N_A molar ratio of 1:40 and reaches the saturated value at N_{EB}/N_A molar ratio above 1:40.

For PANI-H_2SO_4/HCOOH, the specific conductivity decreases at N_{EB}/N_A molar ratio greater than 1:40 due to the change in the morphology from fibrillar to globular. This is because the increase in the intramolecular H-bonding during the deprotonation process, resulting in entanglement of polymer chains and therefore the globular shape occurred. The mechanism is explained in Scheme 4.3.

4.2.2 Effect of % Bipolaron and % Polaron on the Specific Conductivity.

According to the equation : $\sigma = \Sigma\ n_i\mu_i\epsilon_i$, n_i is the number of charge carriers of species, ϵ_i is the charge on each carrier, and μ_i is carrier mobilities , the numbers of % bipolaron and % polaron which relate to the number of carrier molecule on the polymer backbone were studied in this work. Percentage of bipolaron and polaron can be calculated from UV-Visible technique (Appendix C). The areas under the benzenoid, bipolaron, quinoid and polaron peak were obtained from using a Guassian equation (4.2) (Tripreuttunya, 1994)

$$(1/(SD*((2*(22/7))^{0.5})))*exp(0.5(((x-avg)/SD)^2))*area_{total} \qquad (4.2)$$

where : SD $\quad$ = standard deviation of areas

$\qquad$ avg $\quad$ = average of areas

$\qquad$ x $\qquad$ = area of each peak.

Figure 4.22 shows the dependence of %Bipolaron +%Polaron on degree of doping . Since fractions of bipolaron and polaron indicating the number of charge carriers directly influence the specific conductivity. The number of charge carriers (#) can be calculated from the following equation:

$\#$ of charge carriers$_{total}$ $\quad$ = # of charge carriers$_{bipolaron}$ + # of charge

$\qquad\qquad\qquad\qquad\qquad\qquad$ carriers$_{polaron}$ $\qquad\qquad\qquad\qquad$ (4.3)

$\qquad$ # of Bipolaron $\quad$ = 2x N x (% Bipolaron) $\qquad\qquad$ (4.4)

$\qquad$ # of Polaron $\qquad$ = N x (%Polaron) $\qquad\qquad\qquad$ (4.5)
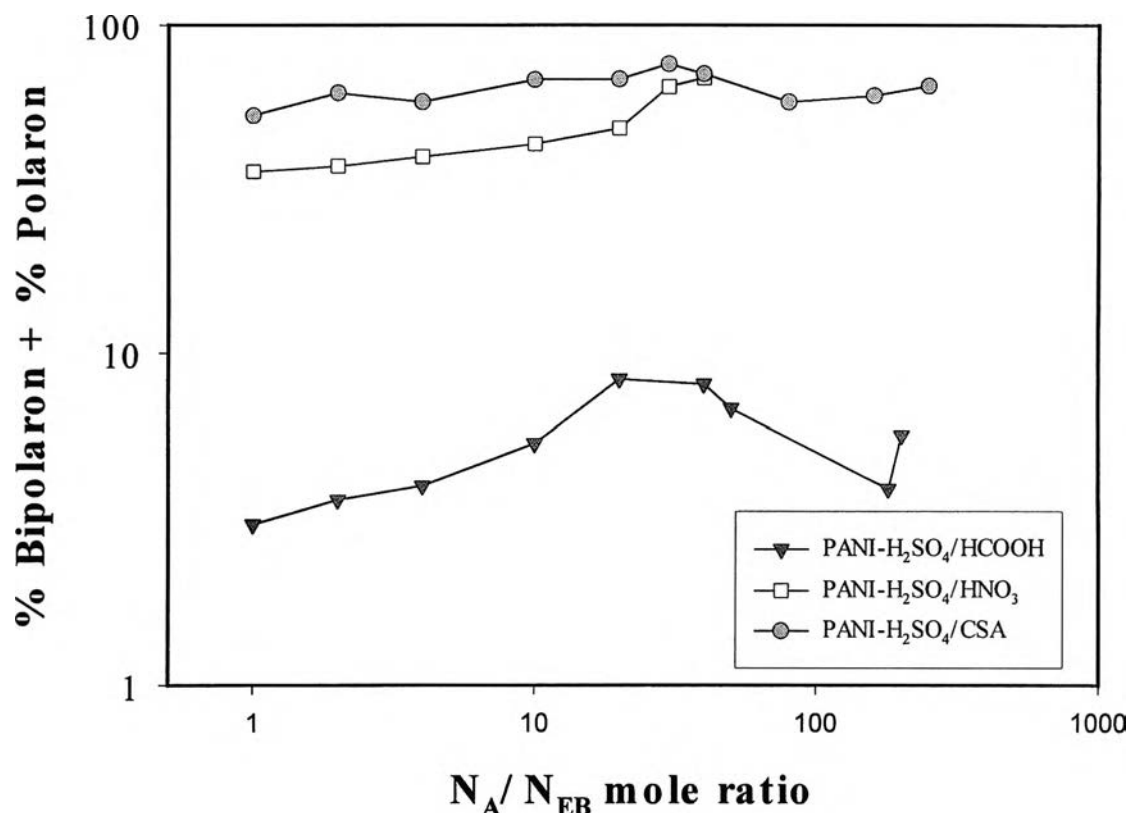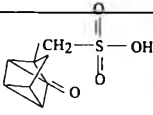
where N is degree of polymerization.

Figure 4.22 The relation between % Bipolaron + % Polaron and specific conductivity.

According to Figure 4.22, % Bipolaron + % Polaron of doped PANI depends largely on the type of acid dopant used and slightly on doping level. It can be seen that PANI-H_2SO_4/CSA has the highest amount of % Bipolaron + % Polaron even at very low doping levels. This is because at the low doping levels used, it has already reached the saturated state. Therefore, amount of % Bipolaron + % Polaron is not largely influenced as doping level is increased. On the other hands, in the case of PANI-H_2SO_4/HNO_3 and PANI-H_2SO_4/HCOOH, % Bipolaron + % Polaron increased substantially as amount of doping level was increased. This can be explained that in the initial state of doping, their % Bipolaron + % Polaron values were far from the asymptotic state.

4.2.3 Effect of Acid Dissociation Constant (pK_a)on the Specific Conductivity.

In order to study the effect of pK_a value on the specific conductivity, three different acid dopants with different in pK_a value were used: HCOOH, HNO_3 and CSA. The pK_a value of each acid dopant is listed in Table 4.8.

Table 4.8 Acid dissociation constant (pK_a).

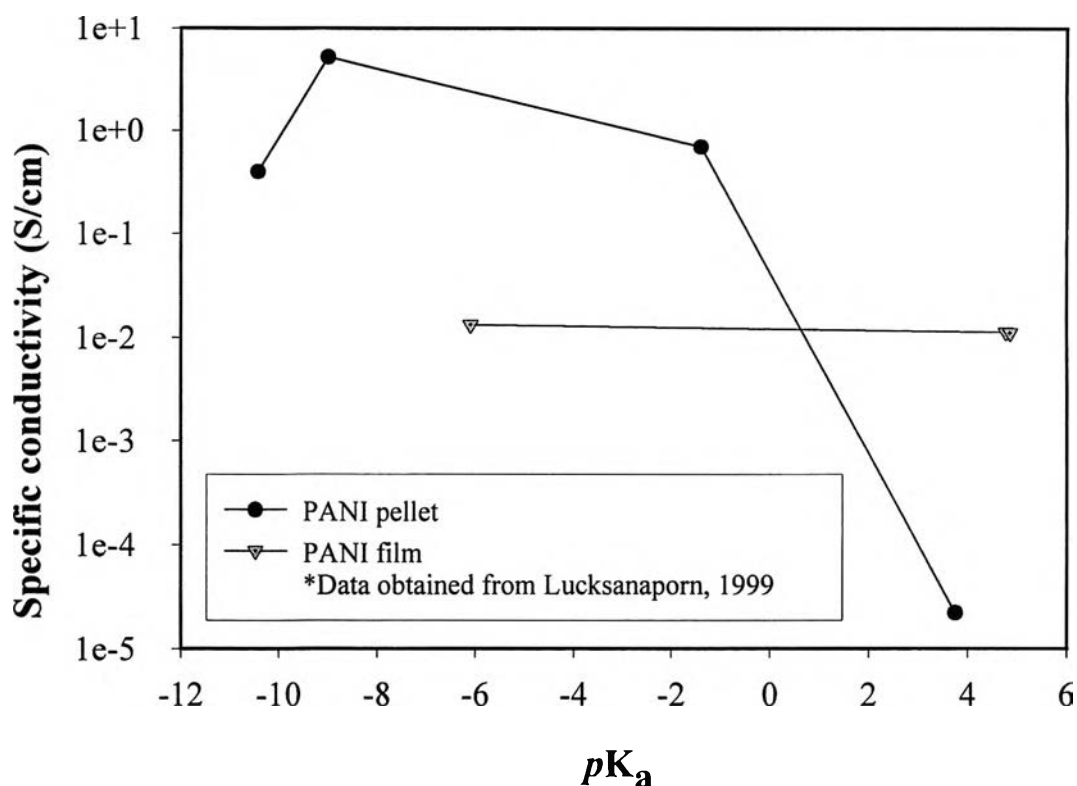| Acid dopant	pK_a value	Structure
1. CSA	-10.43	
2. HBr	-9	H-Br
3. HNO_3	1.4	$H-NO_3$
4. HCOOH	3.75	H- C -OH O

Figure 4.23 Effect of $p\text{K}_a$ value on the specific conductivity.

Figure 4.23 shows the relation between $p\text{K}_a$ value and specific conductivity at the saturated state. Acid with a lower in $p\text{K}_a$ value also gives a lower specific conductivity. This result suggests that it has a lower efficiency to protonate H^+ at N imine sites. This results in a lower degree of doping level and also specific conductivity. However, from the graph, it can be seen that HBr and HNO_3, having higher $p\text{K}_a$ values than CSA, have higher specific conductivity. This can be explained by the sizes of counter ions of both HBr and HNO_3 which are smaller. So, the ability of the acids to protonate at N imine sites is higher than in the case of CSA. Therefore, it can be concluded that the specific conductivity depends not only on $p\text{K}_a$ value but also the structure and size of each acid dopant.

4.2.4 The Specific Conductivity of Polyaniline Pellets when exposed to 100% Ethanol

Specific conductivity values of polyaniline pellets were measured by using the four-point probe under atmospheric pressure, $60\pm 5\%$ relative humidity and $28\pm 2°C$.
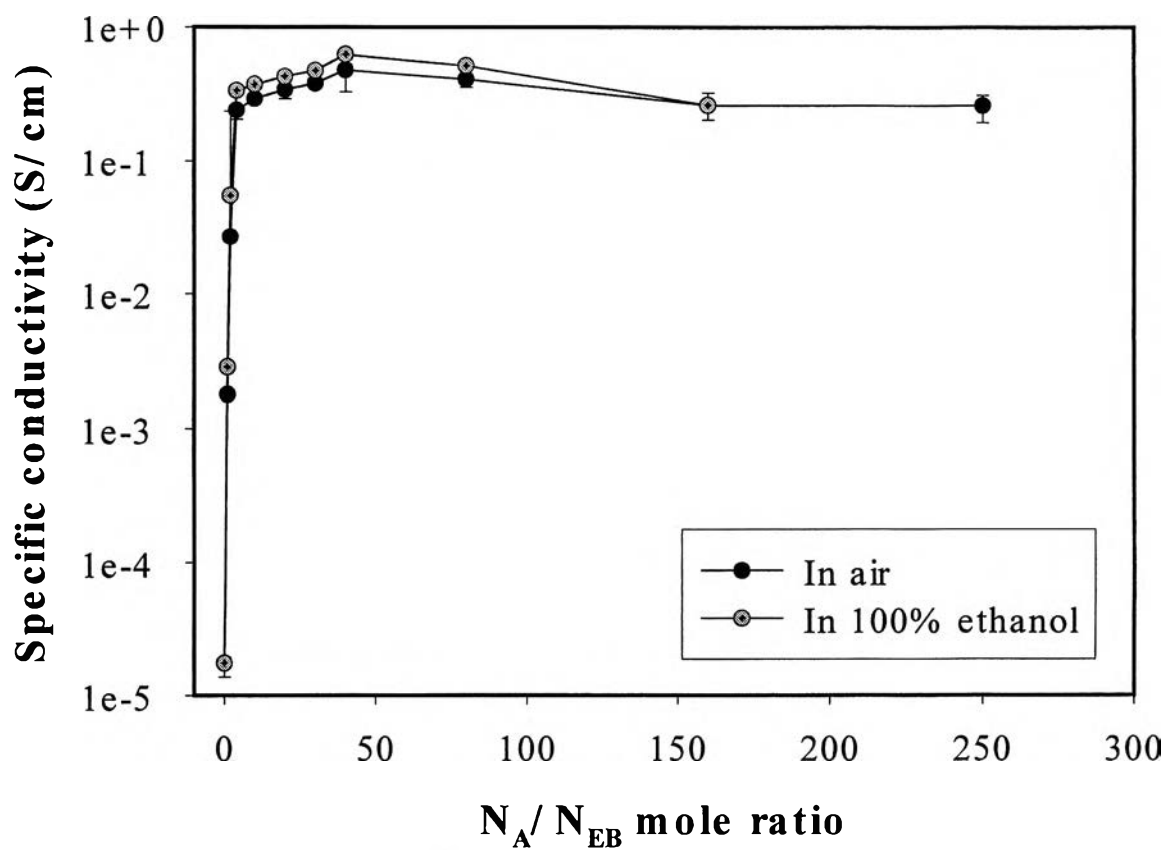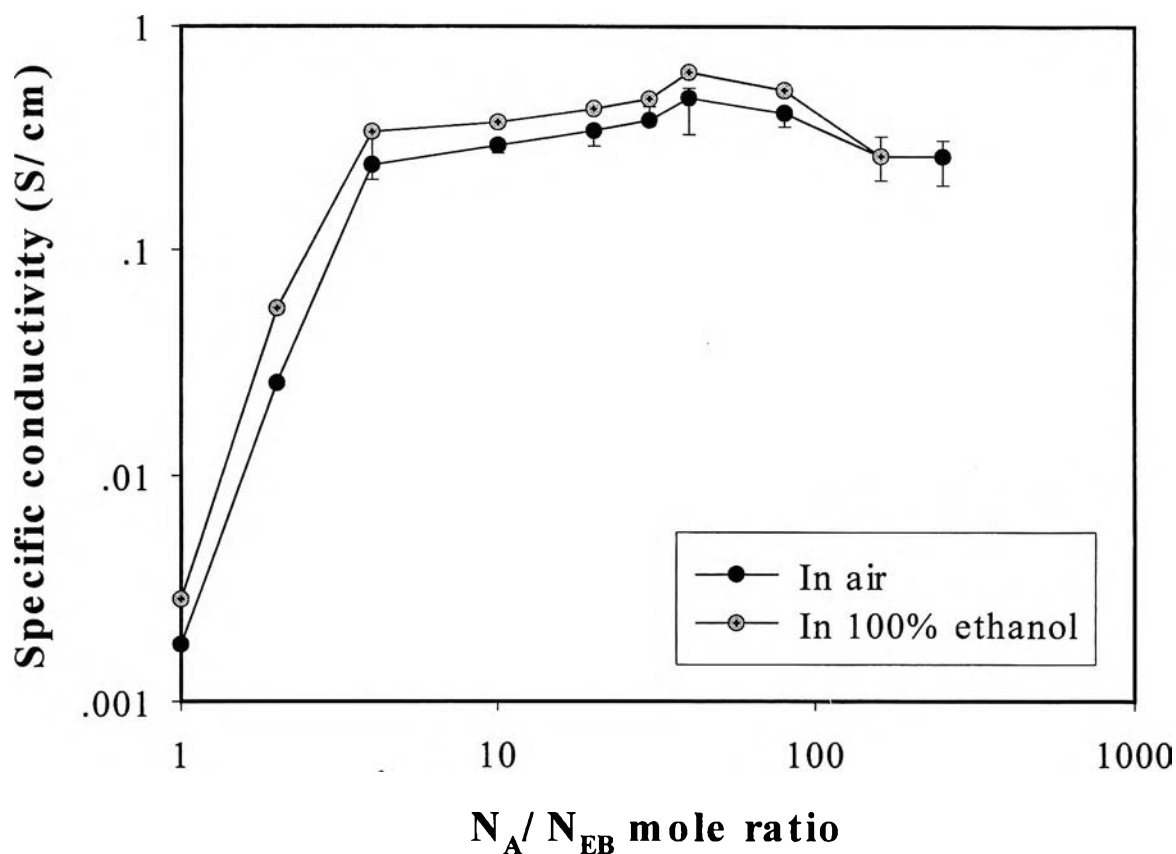
Figure 4.24 The specific conductivity of PANI-H$_2$SO$_4$/CSA in air and in 100% ethanol under the condition of 1 atm, 60± 5%relative humidity and 28 ± 2°C.

Figure 4.24 illustrates the specific conductivity of PANI-H$_2$SO$_4$/CSA in air and in 100% ethanol at various N$_{EB}$/N$_A$ ratios. It shows an increase in specific conductivity when exposed to 100%ethanol. This result was due to the increase in the interchain H$^+$ transfer (MacDiarmid and Epstein, 1989); ethanol molecule acted as a carrier to transfer H$^+$ from a polymer chain to another as shown in Scheme 4.4. Some quinoid segments were protonated resulting in an increase in positive charges on the polymer chain and therefore electrons can delocalize along the chain more effectively. From the equation: $\sigma = \Sigma\mu_i \, n_i \, \varepsilon_i$, the specific conductivity (σ) is proportional to the charge mobility (μ_i). When

protons (H$^+$) are transferred, the mobility of charges increases, and hence an increase in the specific conducitvity.

chain I

chain II

chain III

chain II

chain III

chain II

chain III
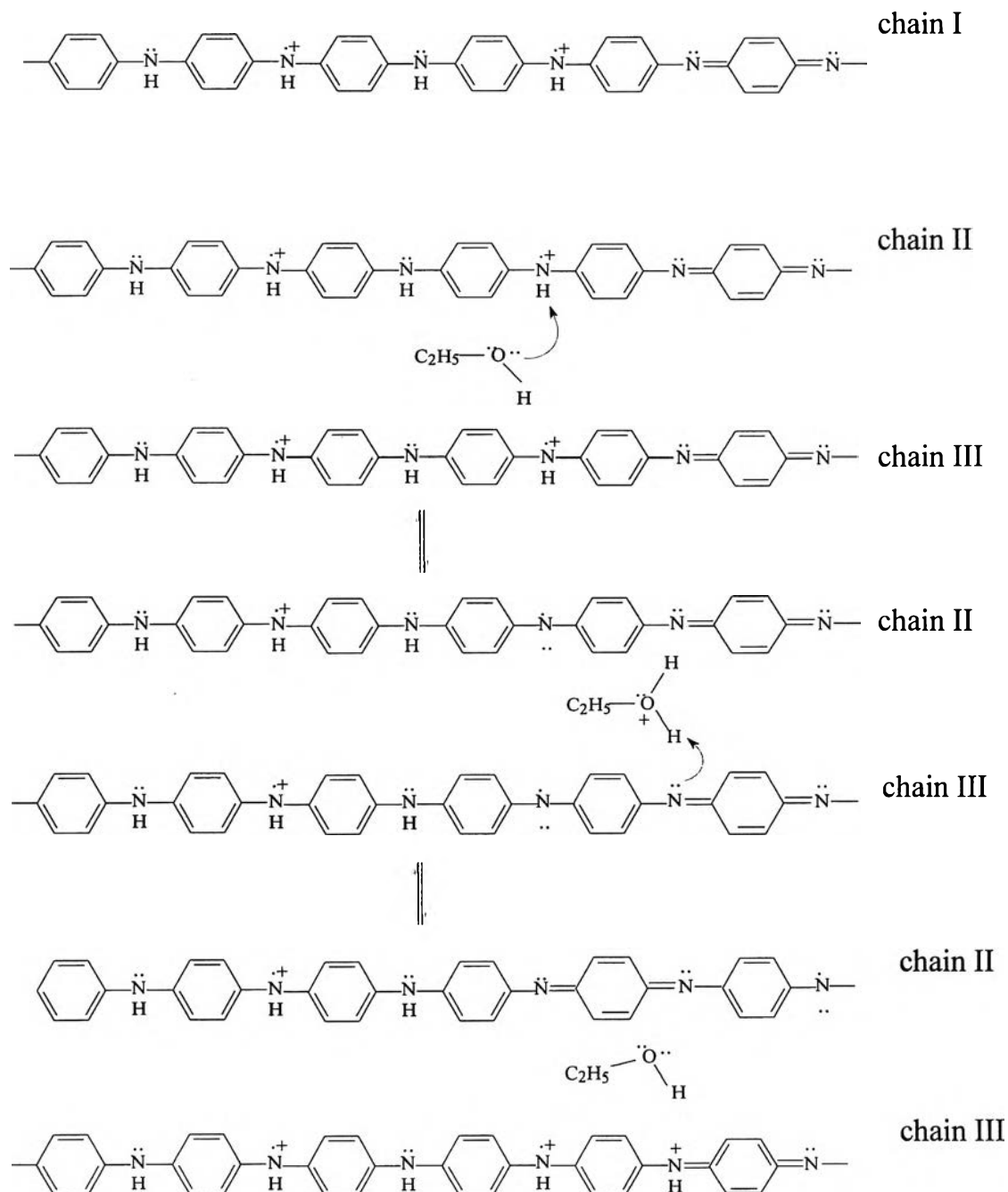
Scheme 4.4 The proposed mechanism of interchain H-transfer when polyaniline pellets were exposed to 100% ethanol.

4.2.5 Sensitivity of PANI-H₂SO₄/CSA to Ethanol Concentration

Typically, the sensitivity can be determined from the slope of the graph of $\Delta\sigma$ and ethanol concentration (%). $\Delta\sigma$ can be found by the following equation:

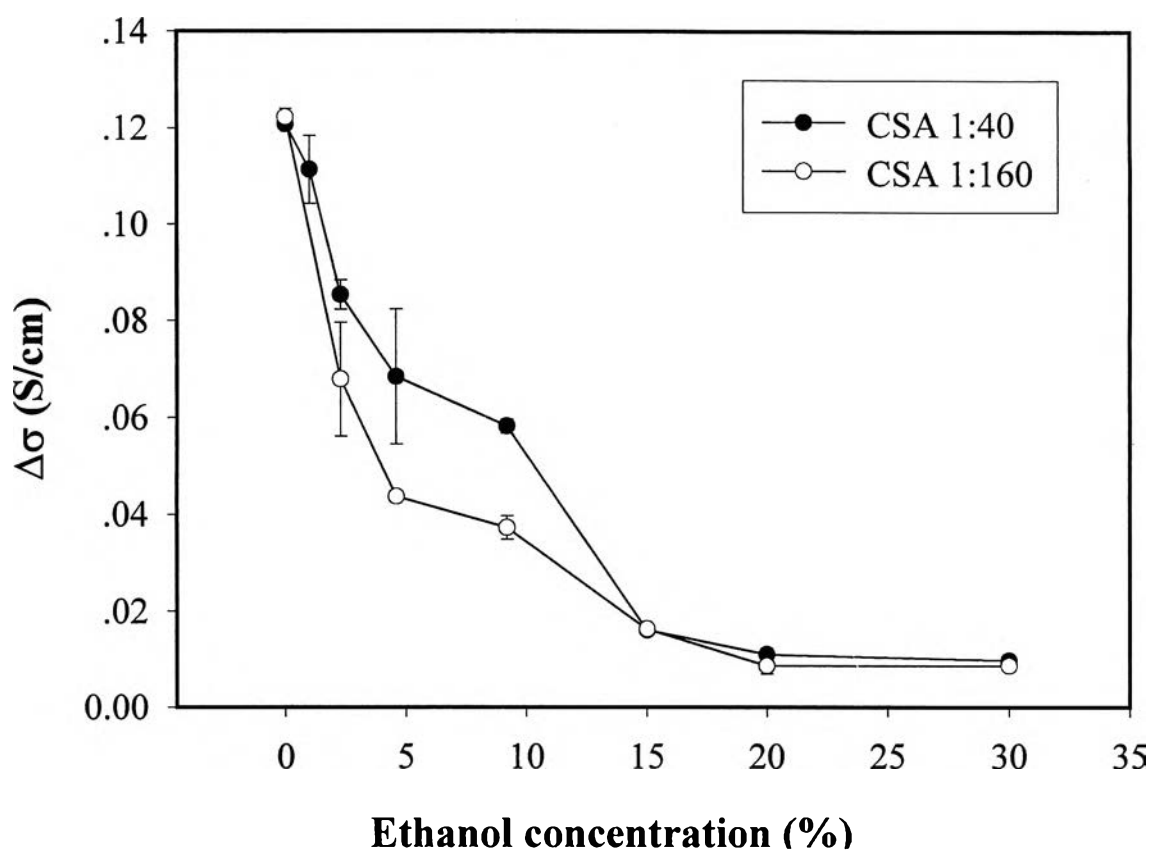$$\Delta\sigma = \sigma_{ethanol} - \sigma_{air} \qquad (4.6)$$

Figure 4.25 Sensitivity of polyaniline pellets after exposed to various ethanol concentration under the condition of 1 atm, $60\pm 5\%$ relative humidity and $28 \pm 2°$ C.

According to the graph, when polyaniline pellets of both PANI-H₂SO₄/CSA at the doping ratios of 1:40 and 1:160 were exposed to 0% ethanol or pure H₂O, they had the highest $\Delta\sigma$ because H₂O molecules served

as carrier molecules. The mechanism occurred similarly for ethanol molecules as shown in Scheme 4.4. As % ethanol concentration increased, the amount of H_2O molecules decreased and the number of ethanol molecules as the carrier molecule increased. We found that specific conductivity decreased. This is because the size of H_2O molecule is smaller than ethanol molecule, so the ability to carry an electron from one chain to another of a H_2O molecule is higher than that of an ethanol molecule.

4.2.6 FTIR Characterization of PANI Before and After Exposing to Ethanol.

The FTIR spectra of PANI before and after exposing to ethanol are shown in Figure 4.26. Polyaniline pellets were ground with KBr and pelletized by using a hydraulic valve press. The sample was pressed under 8 kg/cm^2 for 2 minute. Then quickly transferred to the FT-IR chamber. Spectra (a) and (b) were obtained from two samples of PANI after exposing to ethanol. According to the Figure, the 5 important peaks remain at the same wave number before and after exposing to ethanol. So, it can be concluded that there is no change in the structure of PANI-H$_2$SO$_4$/CSA after exposing to ethanol.
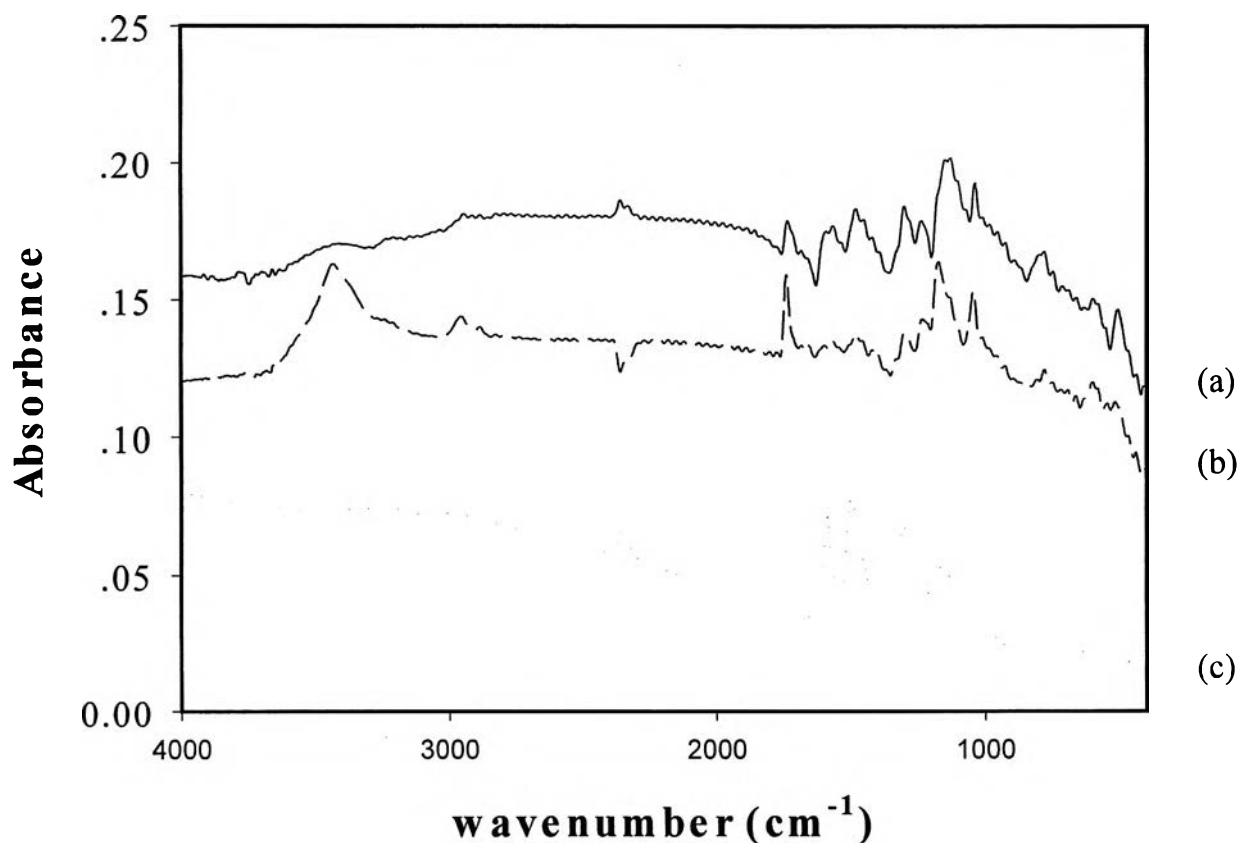

Figure 4.26 FTIR spectra of PANI-H$_2$SO$_4$/CSA: (a), (b) after exposing to ethanol ; and (c) before exposing to ethanol.